CYCLOSTRATIGRAPHY AND CHRONOLOGY OF THE ALBIAN STAGE (PIOBBICO CORE, ITALY)

ALESSANDRO GRIPPO
Department of Earth Sciences, University of Southern California, Los Angeles, California 90089-0740, U.S.A.
e-mail: grippo@earth.usc.edu
ALFRED G. FISCHER
Department of Earth Sciences, University of Southern California, Los Angeles, California 90089-0740, U.S.A.
LINDA A. HINNOV
Department of Earth and Planetary Sciences, Johns Hopkins University, Baltimore, Maryland 21218, U.S.A.
TIMOTHY D. HERBERT
Department of Geological Sciences, Box 1846, Brown University, Providence, Rhode Island 02912, U.S.A.
AND
ISABELLA PREMOLI SILVA
Dipartimento di Scienze della Terra, Università di Milano, via Mangiagalli 34, 30133 Milano, MI, Italy

Abstract: The mid-Cretaceous (Albian) deep-water sediments (coccolith–globigerinacean marls) of the Umbria–Marche Apennines show complex rhythmic bedding. We integrated earlier work with a time-series study of a digitized and image-processed photographic log of the Piobbico core. A drab facies is viewed as recording normal stratified conditions, and a red facies as the product of downwelling warm saline (halothermal) waters. Both are pervaded by orbital (Milankovitch) rhythms. These reflect fluctuations in the composition and abundance of the calcareous plankton in the upper waters. The drab facies is overprinted by redox oscillations on the bottom, including episodic precessional anaerobic pulses (PAPs). Contrasts between the individual beds representing the alternate phases of the precessional rhythm rose and fell with orbital eccentricity, in the classical pattern of Berger's climatic precession or precession index curve, varyingly complicated by the obliquity rhythm. We conclude that greenhouse oceans in general, and perhaps this area in particular, were very sensitive to orbital forcing. Our count of 29 406-ky eccentricity cycles yields an Albian duration of 11.8 ± 0.4 My.

INTRODUCTION

The Umbria–Marche arc of the Apennines, in the region west of Ancona, contains a continuous history of pelagic–hemipelagic sedimentation extending from Early Jurassic times into the Miocene (Cresta et al., 1989). It is here (at Gubbio) that the impact nature of the Cretaceous–Tertiary boundary was discovered, and that continuous stratigraphic profiles of Cretaceous–Paleogene magnetic zonation were developed. The Cretaceous biostratigraphy of the region is summarized in Premoli Silva and Sliter (1995).

The Albian Stage is here represented by 50–60 m of pelagic sediment, initially coccolith–globigerinid ooze and marl, now compacted into rhythmically alternating beds of marlstone and limestone that form the Scisti a Fucoidi (Fucoid Marls) and the basal beds of the succeeding Scaglia Bianca Limestone.

History of Study

The rhythmicity was first studied in discontinuous outcrops by de Boer (1982,1983) and de Boer and Wonders (1984). A stratigraphic thickness of 50–60 m, representing a stage with an estimated duration of ca. 12 million years, implies a mean accumulation rate of 4–5 Bubnoff units (mm/ky, m/My). That made the ca. 8 cm bedding couplets likely candidates for the precessional cycle, and their grouping into bundles of five a likely expression of the short-eccentricity cycle. Schwarzacher and Fischer (1982) had reached similar conclusions about cyclic patterns in the underlying Barremian and overlying Cenomanian limestones.

Continuity of sequence was obtained in the Piobbico core, drilled by Premoli Silva, Napoleone, and Fischer through the Scisti a Fucoidi at the Le Brecce farm northwest of Piobbico (Fig. 1). Pratt and King (1986) described the composition of the organic matter. Detailed studies mainly directed at an 8 m core segment (cycles 8–12, Fig. 16) yielded calcium carbonate profiles and a gray-scale scan by densitometry of diapositives (Herbert and Fischer, 1986, Herbert et al., 1986). These yielded new insights into rhythmicity and sedimentation, and the gray-scale scan showed reflectivity to be an excellent proxy for calcium carbonate content, save for a step function from gray to black associated with black marlstone beds (the PAPs of this paper). Spectral studies by Park and Herbert (1987), Premoli Silva et al. (1989a), and Premoli Silva et al. (1989b) confirmed the assignment of cyclicities and discovered the presence of an obliquity signal. The stratigraphy of the core was described by Erba (1988) and Tornaghi et al. (1989).

The chemical and gray-scale analyses employed had proved too tedious for large-scale application to cyclostratigraphic studies. The visual count of the short-eccentricity bundles in core and outcrop by Herbert et al. (1995) yielded an Albian duration of 11.9 My, but it remained undocumented.

By then, digitization of photographs and programs for time-series analysis had brought the entire core into reach of study and documentation. Fischer and Grippo, with the aid of Hinnov, undertook a restudy of the core photographs (for details, see Appendix). By means of a photolog, gray-scale log, and spectral analyses we were able to document the cyclicity in the ca. ten million years of history recovered by the core, and we extended this to the full Albian by extrapolation to the surface data of Herbert et al. (1995).

While these studies were in progress, Fiet et al. (2001) measured a surface section of the Albian on Monte Petrano, some 13

Cyclostratigraphy: Approaches and Case Histories
SEPM Special Publication No. 81, Copyright © 2004
SEPM (Society for Sedimentary Geology), ISBN 1-56576-108-1, p. 57–81.

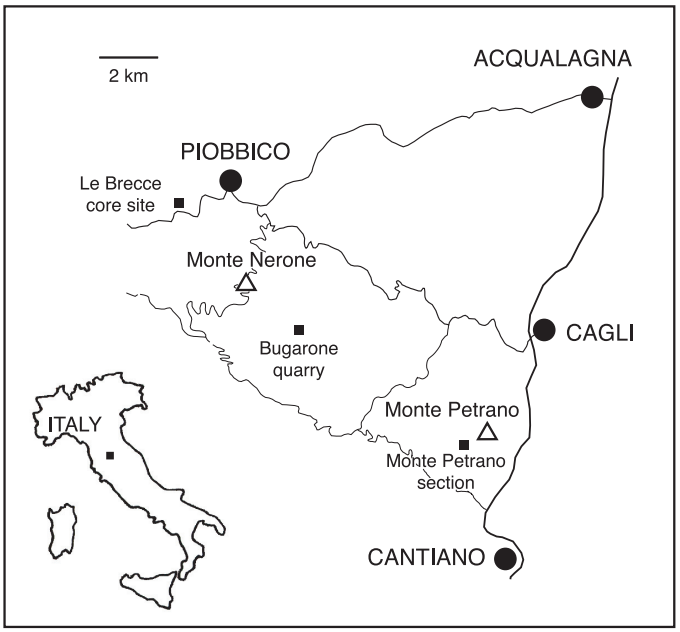

FIG. 1.—Index map.

km to the southeast of our drill site. Although some distinctive lithic and faunal markers provide a general correlation, an overall cycle-to-cycle correlation is not achieved, though in the end their assignment of 11.4 My to the Albian is only one 406 ky cycle short of ours.

Conventions

We here use the terms *cyclicity* or *rhythm* for the general process that, plotted through time, appears as a wave train, and we reserve *cycle* for the individual wave.

The need to refer to individual cycles made it necessary to devise a system of numeration. Superbundles corresponding to 406 ky eccentricity E-cycles are numbered from the top of the Albian downward (Figs. 4, 15, 16), and bundles for each superbundle are lettered a, b, c, d in upward progression. The core begins in cycle 3. Spectral coverage extends from the top of cycle 8 downward, and the base of the Albian lies somewhere between the upper part of cycle 29 and the lower part of 31, and is tentatively placed in cycle 30 (Fig. 15).

We give radiometric age estimates in kiloyears and million years as ka and Ma, and stratigraphic ones, including those derived with astronomic help, as ky and My.

SCISTI A FUCOIDI

The Scisti a Fucoidi represent coccolith–foraminiferal marls, comparable to modern marly globigerinid ooze, deposited at a depth estimated at ca. 2 km (Premoli Silva and Sliter, 1995).

The mean accumulation rate (compacted) was on the order of 4 Bubnoff units (mm/ky, m/My). Restriction of calcareous fossils to those initially calcitic indicates deposition below aragonite compensation level but generally above the calcite lysocline.

All of the Tethyan foraminiferal and nannofossil zones of the Albian are represented, and deposition is thought to have been essentially continuous (Premoli Silva and Sliter, 1995), extending from its base in the overlap between the nannofossil *Predicosphaera columnata* and the foraminiferal *Hedbergella planispira* zones, to its top at the base of the *Rotalipora brotzeni* zone.

Sedimentation

Our understanding of sedimentation goes back to the observations of de Boer (1982, 1983) and the study of an 8 m segment (our cycles 8–12) by Herbert and Fischer (1986) and Herbert et al. (1986), supplemented by other observations in outcrop and on the core (e.g., Tornaghi et al., 1989).

The initial sediment consisted mainly of coccoliths, planktonic foraminifera, a minor phase of biogenic silica partly or wholly attributable to radiolarians, and terrigenous siliciclastic matter (probably eolian dust) (de Boer, 1982, 1983; de Boer and Wonders, 1984; Herbert and Fischer, 1986; Herbert et al., 1986). The dust supply appears to have been comparatively constant, whereas the supply of skeletal calcite fluctuated, in rhythmic fashion, to yield stratification. Beds are planar, and bedding planes are generally not sharply defined but gradational. The more calcareous beds contain, at odd intervals, centimeter-scale lenses of cross-bedded radiolarite, representing ripple-drifted radiolarian ooze. In these the tests have largely been calcified while the silica moved to fill the interior as chalcedony. (Fischer, personal observations). Excess silica in the limestones suggests that biogenic silica, generally not visibly preserved, fluctuated along with carbonate (Herbert et al., 1986).

These findings, based on detailed study of parts of the sequence, appear applicable to all of it, but are in no sense complete, and our interpretations thus remain generalized. Isotopic records are strongly overprinted by pervasive calcite cement.

While thus relatively simple in basic constituents, the stratigraphic sequence is dramatically differentiated in color, ranging from greenish gray to white, to black, and to red (Figs. 2, 4), in response to wide fluctuations in depositional redox conditions.

Drab Facies.—

Most of the sequence takes the drab form (Fig. 2). Greenish-gray beds of marlstone grade on the one hand into limestones, whitish by virtue of the reflectance of calcite. On the other hand, the greenish marls grade into thin black marlstones colored by organic matter and iron sulfide, and representing precessional anoxic pulsations (PAPs).

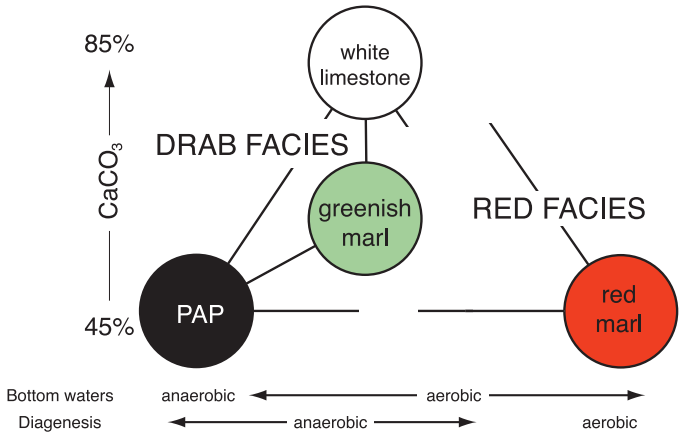

FIG. 2.—Lithic phases and inferred aeration states.

Carbonate Oscillations.—The initial calcite constituents were of two main sorts: coccoliths, and planktonic foraminifera. The purest limestones are composed mainly of coccoliths, planktonic foraminifera being suppressed in numbers and restricted to smaller, simpler forms (hedbergellids). Planktonic foraminifera reach greatest abundance and diversity in the gray-green marls and PAPs, where they attain the full complement of the Tethyan faunas, including the large and more highly ornamented species (Premoli Silva et al., 1989a; Premoli Silva et al., 1989b).

Bioturbation.—Our information on bioturbation is based on observations by Erba and Premoli Silva (1994), confined largely to cycles 8–12, but appear applicable to the entire sequence by general observations in the field and on the core. The ichnofauna lacks the largest bioturbators such as *Thalassinoides*, probably because of water depth, but it contains *Chondrites* (the "fucoids" from which the formation derives its name), as well as *Teichichnus* and *Zoophycos*. Varied in the more calcareous beds, it becomes restricted to *Chondrites* in the more clay-rich members and tends to dwindle to small *Chondrites* at the boundary with PAPs.

The variation in ichnofauna thus parallels that found by Savrda and Bottjer (1994) in the Niobrara Formation in Colorado. There, diversity of ichnofauna, size of burrows, and diversity of shelly benthos are associated with oxygenated seafloors of the carbonate facies. They decline to *Chondrites* in the dysaerobic shales and are lacking in the anaerobically deposited black shales. It would appear that the limestones in the Scisti a Fucoidi were deposited on moderately well aerated bottoms, which turned dysaerobic with the deposition of the greenish marls.

Precessional Anoxic Pulsations (PAPs).—Episodic intensification of this redox oscillation produced anoxia or near-anoxia as recorded in black marls, which may occupy part or all of the marly bed. These PAPs have generally been referred to as black shales, but, lacking fissility and retaining considerable carbonate, are marlstones. Their carbonate content averages lower than that of the greenish-gray marls (Herbert and Fischer, 1986), owing to a reduced content of coccoliths (Erba, 1988, 1992). The organic-matter content generally lies in the 1–2% range, and the intensity of pigmentation suggests presence of elemental carbon, supplemented by iron sulfides (de Boer, 1983; Herbert and Fischer, 1986). The average hydrogen content of the organic matter is generally low, and the abundance of wax-derived n-alkanes in the extractable compounds (Pratt and King, 1986) suggests that soot may constitute up to 50% of the organic fraction. Lack of fine laminations implies mixing on a microscopic scale, implying dysaerobic episodes when small nektonic animals may have disturbed the bottoms or when very small benthonic ones obtained temporary footholds.

Urbino Anoxic Event.—Distinct from the PAPs is the Urbino marlstone bed in our cycle 27 (Fig. 16). In this, persistence of anaerobic conditions formed a 40 cm bed of thinly laminated black marlstone. In persistence of anoxia and in its high organic and hydrogen content (Pratt and King, 1986) it resembles the Selli (OAE1a) unit of the lower Aptian and the Bonarelli (OAE2) unit of the uppermost Cenomanian, but unlike these it contains considerable calcite in the form of recrystallized laminae of planktonic foraminifera, and it is not cherty. It appears to represent an appreciable fraction of a 406 ky eccentricity cycle, an episode of prolonged anaerobic conditions. Its timing is roughly that of OAE1b, but its identity with this remains in doubt.

Red Facies.—

The red facies also consists of coccolith–globigerinid marls, showing a similar rhythmicity in oscillating carbonate contents and foraminifer/coccolith ratios, but its carbonate values remain below those attained in the drab facies. The redox cycle is generally lacking; these sediments were deposited in well-aerated water, in which all of the reactive iron minerals were converted to the ferric form. Furthermore, little or no reactive organic carbon was buried, so that the iron remained ferric through diagenesis. The degree of redness varies, there being a gradation from greenish gray marls through units tinged by pink and lavender, as in cycle 13 (Fig. 4, 16), to bright red marls and (rare) decalcified maroon mudstones. The amplitude of carbonate variation is reduced from that shown in the drab facies, and PAPs are missing except for a few in the transitional facies.

The red facies is also set apart by lack of bioturbation. In the drab facies the vigor and diversity of bioturbators grew with oxygen supply. One might thus expect the red facies to show an even more diverse ichnofauna, with conspicuous large burrows, but this is not the case. No conspicuous burrows were noted in field and core (Fischer, personal observations). The sediments are not conspicuously laminated, suggesting that mixing occurred on a fine scale, but the common presence of individual fine foraminiferal laminae with centimeter and sub-centimeter spacing implies little large-scale burrow mixing. We conclude that macroburrowers, abundant at this depth in the flysch facies, were scarce on these bottoms, limited not by oxygen but by scarcity of food.

Condensed Mudstones.—A variant of the red facies is represented by maroon mudstones, condensed zones of carbonate dissolution in the lower part of the succession. They lack microfossils and appear to be dissolution zones, stratigraphically condensed.

The red–drab alternations seem unrelated to the pattern of orbital variations.

NEW CORE SCAN

The Piobbico core (Fig. 1, 16) was drilled in 1982 on the Le Brecce farm some 2 km west of Piobbico on the road to Apecchio (Tornaghi et al., 1989). It yielded 44 m of Albian strata, missing the uppermost 6 m. It obtained excellent recoveries except for gaps in its uppermost 5.5 m, and missed 2 m of the middle Albian cut out by a fault (Herbert et al., 1995) (Fig. 16).

Soon after drilling, the core was split by diamond saw and divided into < 30 cm segments. Those of the archive set were embedded in plastic and smoothed with 600 mesh carborundum. Acetate replication of this surface after a light etch by hydrochloric acid provided microscopic access to the entire core, allowing precise delimitation of biostratigraphic zones. Each of these segments was photographed on Ektachrome film, with submillimeter resolution. These pictures served as the basis for the new analysis.

Scans and Logs

Our return to the Piobbico core was motivated by the desire to test more rapid yet quantitative techniques for extracting and processing cycle information. Digitization of pictures, and software for rapid gray-scale scanning and time-series processing, allowed us to undertake a reanalysis (for details, see Appendix).

Photolog.—

We digitized the pictures and cleared a path across each of nonstratigraphic information. We concatenated these paths into a single stratigraphically continuous scanning path, the consecutive pixels of which form, in theory, a historical series of observations (samples). This, the colored series, was corrected for dip to true stratigraphic depth and printed as a *photolog* (Figs. 4, 16A), with a pixel density equivalent to 6 mm of rock.

Gray-Scale Series.—

We then converted the colored series into a gray-scale series that served as the basis for subsequent calculations. Small gaps due to incomplete recovery render the upper 5.5 m unsuitable for detailed analysis, but from this point down the entire record was analyzed, with exception of the two meters excised by the fault.

Gray-Scale Log.—

The gray-scale series can be printed out as a gray-scale log, which, for greater visual impact, we present in mirrored form (Figs. 4, 16B). The convention we chose was to mirror the plot on black, so as to spread the limestones and contract the PAPs, which thus come to segment the image into the ca. 40 cm bundles. The cyclicity can be pictured in quite the opposite way (Fig. 13 B), with white in the center, contracting limestones and expanding the PAPs into spikes.

Power Spectra

In order to obtain a more objective view of the cyclicities we turn to the frequency domain of power spectra. We employed tapered Thomson spectra, well adapted for study of irregularly time-sampled series.

The spectrum of the entire scan (Fig. 3A) shows groups of peaks, at certain stratigraphic spacings. Peaks concentrated at the extreme (low frequency) left have little significance ("red noise" enhanced by the logarithmic scale). The group in the 30–60 cm bracket corresponds to the stratigraphic bundle, identified by de Boer (1982), Herbert and Fischer (1986), and Park and Herbert (1987) with the 95 ky eccentricity cycle. The prominent peak at ca. 20 cm corresponds to no stratigraphic feature observed in field or core, but to the obliquity cycle found spectrally by Park and Herbert (1987) and Premoli Silva et al. (1989b). A scattering of peaks in the 9–14 cm region corresponds to the couplets identified by the same authors with the two precessional modes. The main periodicities in this spectrum are thus consonant with those previously found and identified as the major elements of the orbital variations,

Tuning.—

The multiplicity of peaks in Figure 3A derives mainly from variations in accumulation rate, i.e., from deviations of the stratigraphic space dimension from time. "Tuning" involves the choice of some consistently recorded cyclicity, whose individual cycles in the data series can be stretched or condensed to the same length, in essence moving them out of the space domain into the time domain. The eccentricity values were taken to be the modern ones, as computed by Laskar for the last 19 My (1999). For obliquity and precession we use the Berger et al. (1989) estimates for 95 Ma, 38.9 ky for obliquity, and 22.3 and 19.5 ky for the precessional mode.

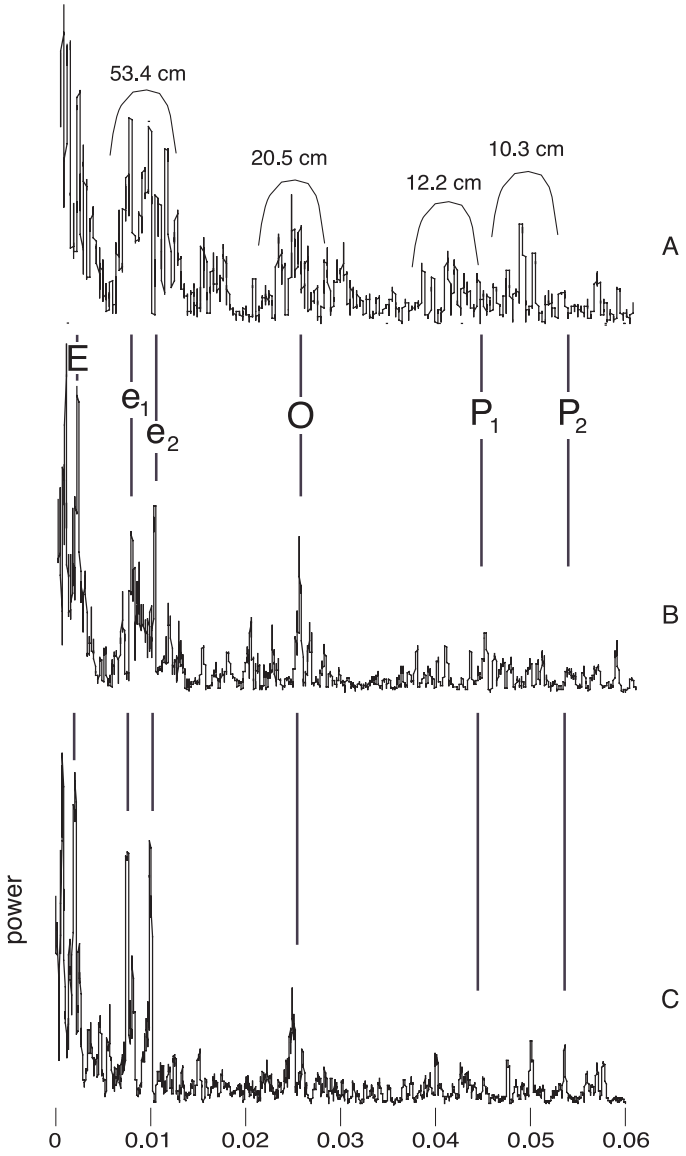

FIG. 3.—Power spectra of full time series. **A)** Untuned spectrum, referred to stratigraphic space. **B)** Spectrum tuned to 95 ky bundle. **C)** Spectrum tuned to 406 ky superbundle or its equivalent. E, predicted 406 ky (long) eccentricity rhythm; e_1 and e_2, predicted modes of the short (ca. 95 ky) eccentricity rhythm; O, predicted obliquity rhythm; P_1 and P_2, predicted modes of the ca. 20 ky precessional rhythm.

Success or failure of tuning can be judged by whether tuning to any one cyclicity helps to align the others or scatters them even more widely, and by whether the resulting alignment of peaks corresponds to the astronomic predictions. Choice of the periodicity to tune to is obviously limited to one that is consistently present and shows well-defined cycle boundaries in the gray-scale log. It should be unimodal, because choice of a bimodal cyclicity would introduce a pseudo-bimodality into the others, particularly those of higher frequency.

The precessional rhythm fails to qualify. The astronomical signal is strongly bimodal, and its preservation in the series is

quite irregular (Figs. 4, 5), with cycles apparently lost to bioturbation and in other cases added by double beats.

The obliquity cycle is very stable in period but is commonly lacking, and its cycle boundaries are masked by interference from the precession–eccentricity syndrome.

The short-eccentricity rhythm is consistently recorded in our series and is thus practical to tune to. The thus-tuned spectrum (Fig. 3B) shows considerable simplification. The peak for the long eccentricity emerges clearly, as do the two modes of the short-eccentricity rhythm. The 20 cm peak is now an excellent match for the obliquity cycle. Couplet peaks remain scattered but show a semblance of two groups corresponding to P_1 and P_2. Some distortion, however, has been introduced by tuning to a bimodal cyclicity.

The long-eccentricity rhythm is very stable at 406 ky, but its sporadic appearance precludes tuning to it directly. But it sets a frame into which the short-eccentricity signals can be fitted. In a complete series, every fourth (occasionally fifth) e-cycle boundary should come close to matching an E-cycle boundary, and this made it possible to extrapolate E-cycle boundaries for the entire sequence, to yield the E-cycle sequence shown in Figures 15 and 16, numbered from the top of the Albian down. This exercise necessitated additions of four previously unrecognized 95 ky cycles, obscured by condensed sedimentation. The resulting spectrum (Fig. 3C) shows further simplification. Peaks for E, e_1, e_2, and O remain aligned with predicted values. The couplet peaks are much simplified from Figure 3B, presumably because no longer doubled by tuning to the bimodal 95 ky cycle, but their fit to the precession estimates is not improved.

Precessional Rhythms

The "precession of the equinoxes" derives from the gyration of Earth's rotational axis. This describes a cone with a period of ca. 25.671 ky relative to the stars. Its influence on climates depends on its interaction with the ellipticity (technically eccentricity) of Earth's (planet 3) orbit. The axis of that orbit, as defined by perihelion (closest approach to the Sun) moves counter to the precessional rotation, cutting the length of the precessional cycle to 19.104 ky. Its orbit is further distorted by the gravitational attractions of Mercury (1), Venus (2), Mars (4), and Jupiter (5), each of which has its own period or frequency, expressed as the sine of its longitude relative to the moving perihelion. Jupiter and Mercury combine to provide a strong precessional periodicity at ca. 23 ky (the P_1 mode) while Earth and Mars combine to form one at ca. 19 ky (P_2). Bracketing the effect of Venus, these modes are commonly thought of as combined into a precessional cyclicity at ca. 21 ky.

As the orbital eccentricity waxes and wanes, it brings changes of insolation that find expression mainly in seasonality. The more circular orbits produce moderate summers and winters. Higher eccentricity brings more intense summer heat and winter cold in the half of the cycle in which perihelion in summer, while during the other (winter-perihelial) half it warms winters and cools summers beyond those of a circular orbit. When perihelion occurs in the summer (and aphelion in the winter), the seasons in that hemisphere are intensified. At the same time those in the other hemisphere are damped. In the succeeding phase these relationships are reversed. The intensity or amplitude of these climatic deviations is proportional to the amount of eccentricity, which varies as described below.

de Boer (1982) and Herbert and Fischer (1986) reckoned that if this Albian sequence of ca. 50 m had been continuously deposited for an estimated 12 My of Albian time, for an accumulation rate of ca. 4 Bubnoff units (mm/ky), then the 6–8 cm couplets would approximately match the precession, and the ca. 30–50 cm bundles would match the ca. 100 ka short cycle of eccentricity. As shown below, the inference is now supported by close comparisons of the spectral signatures.

The "elementary cycle" is one of ca. 8 cm *couplets* that record a pulsation in the rate of carbonate production, attributable to variations in the vigor of coccolithophoracean algae in the photic zone. Not only did the vigor of coccolith blooms vary, but so did the composition of the flora, with species thought to be diagnostic of higher fertility (upwelling) confined to the more calcareous beds (Erba, 1992).

This cyclicity pervades both the drab facies and the red facies. In the drab facies it is joined by a variation in redox conditions on the sea floor. The more calcareous beds show strong bioturbation in which *Zoophycos* and *Planolites* play a role, evidence of moderately good aeration. In the marly members the ichnofauna became restricted to *Chondrites*, indicating dysaerobic conditions, and at times reached anoxia in precessional anoxic pulsations (PAPs) evidenced by black coloration.

In the gray-scale log the precessional couplets appear as high-frequency serrations (Figs. 4, 5, 16). Strength and regularity of the couplets vary, with PAPs deeply segmenting the gray-scale curve. Some couplets have been amalgamated by bioturbation (Fig. 5). In the red facies the couplets show a lower-amplitude variation than in the drab, corresponding to a lesser contrast in carbonate content. In decalcified condensed maroon clays (in cycles 27, 29, and 30) the precessional couplets are wiped out. On the other hand, the transitionally red marls of cycles 13 and 14 preserve the number of precessional couplets most faithfully, owing to the smaller degree of bioturbation (Fig. 5).

Occasional couplets or groups of couplets have a bifid signature, suggesting a precessional double beat previously noted in the precessional cycles at low latitudes, where the counterphased precessional cycles of the two hemispheres interact (Park et al., 1993).

As described above, the decrease in deep-water oxygenation at times became intensified to the point of anoxia, so that part or all of this marl bed turns black, with elevated organic content and iron sulfide. These thin precessional anoxic pulsations (PAPs) segment the stratal sequence in an eye-catching manner (Figs. 4, 16). Their cyclic distribution (Fig. 13) is discussed below. Ash-gray (rather than greenish-gray) beds, shown in Figures 4 and 16, appear to represent relicts of such PAPs. Seasonal anoxia may have produced an alternation of anoxic and aerated times that, with gentle bioturbation in the aerated intervals, yielded a mixed product. But even black marls one to two centimeters thick were threatened by subsequent bioturbation, as shown in outcrop, where, in the Monte Petrano section, a PAP was laterally terminated by dense *Chondrites* burrowing from above (Fischer, personal observations). Either process could readily have left enough carbon particles in the resulting sediment to give it a distinctive ash-gray color. We speak of such beds as inferred PAPs.

The tuned spectrum (Fig. 3C) does indeed show a group of peaks in the estimated precessional spectral band, but these are scattered as compared to the peaks for eccentricity and obliquity. When examined in smaller time slices (Fig. 6), about half of the spectra show two well-defined peaks, in some characteristically paired into the two modes, but slightly displaced toward higher and lower frequencies. The tuning did not, of course, correct for distortions by variations in accumulation rate at frequencies beyond the 406 ky level. Existence of such uncorrected variations is demonstrated in Figure 8. Here individual 95 ky eccentricity bundles show time distortions of a factor of two, much larger than

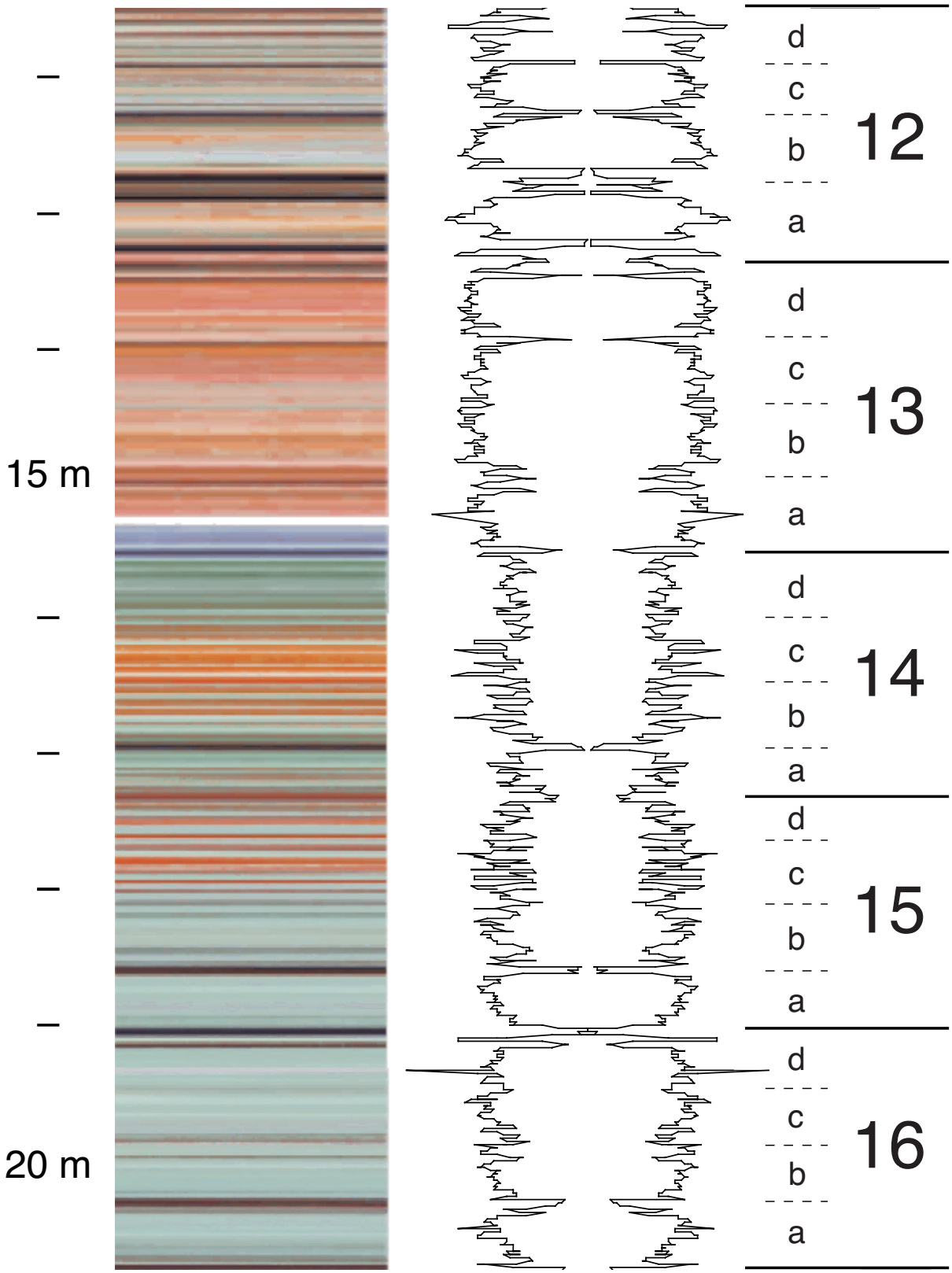

FIG. 4.—Photolog and gray-scale log of a ca. 2 My section of core, comprising superbundles 12–16. Gray-scale scan shown as butterfly plot, from black in center to white (limestone) on margins. Numbers refer to superbundles (406 ky eccentricity cycles), numbered from top of Albian downward. The constituent bundles (95 ky cycles), lettered, a–d, are punctuated by single or groups of precessional black pulses (PAPs). Bundles b and c have become wholly confluent in cycle 13.

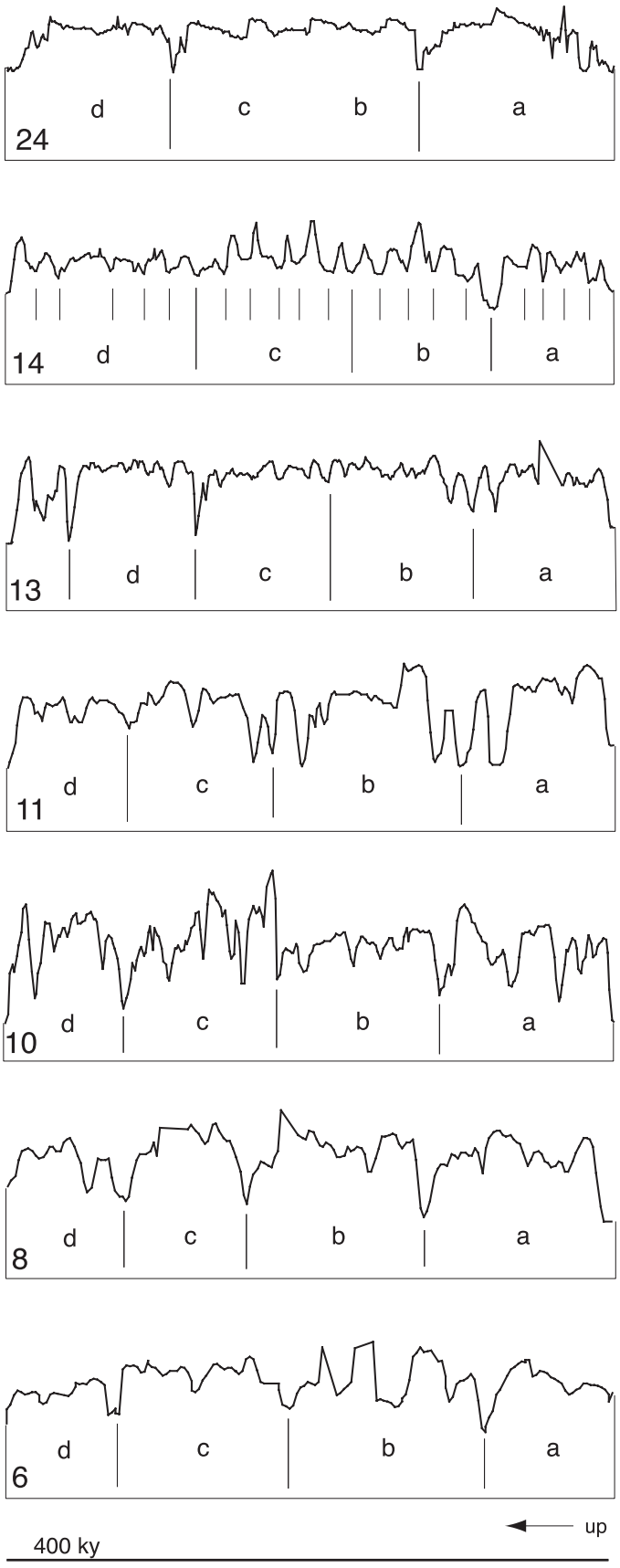

the actual variation in their period. Variations below the 95 ky level could only add to this distorting factor. It nevertheless seemed desirable to test the assignment of the couplets to precessional forcing, in another way.

Precession Confirmed.—

The 10 My duration of the Piobbico series provides an opportunity to investigate the orbital modulations during the mid-Cretaceous. Below we assess the evidence as follows (procedures after Hinnov et al., 2002). (1) isolation of the individually recorded orbital parameters by bandpass filtering; (2) estimation of amplitude modulations of the filtered series using quadrature signal analysis; and (3) spectral analysis of the amplitude modulations and comparison with those of the predicted orbital parameters.

To establish the presence of precessional forcing in the Piobbico series, we filtered the precession band of the tuned series and looked for amplitude modulations matching Earth's orbital eccentricity (following Shackleton et al., 1999; Hinnov, 2000). Because the eccentricity is intact in the tuned series, the amplitude modulations of any existing precession signal should also be intact, despite rate-induced time misalignments in the underlying precession cycles.

The filtered series is shown in Figure 7A. Remarkably, the spectrum of the AM series (Fig. 7B) reveals the clear presence of E, and doublets e_1 and e_2 at frequencies comparable to those observed in the eccentricity band of the tuned series (cf. Fig. 7D). As with the short eccentricity of the tuned series, the AM components interpreted as e_1 and e_2 are centered on frequencies that are slightly red-shifted relative to those of theoretical eccentricity (compare Figs. 7B, D; Table 1B). They match a similar shift in the eccentricity periods measured by us (Fig. 10). In sum, these results confirm that precession forcing played a decisive role in the cyclic sedimentation of the Piobbico series, as has long been hypothesized.

Most of the precession power (Fig. 7A) is concentrated in the PAPs-rich intervals (cycles 8–12 in Figs. 4 and 16). This irregular spacing of amplitude anomalies may preclude detection of the long-period eccentricity patterns sought for. This may explain why the AM series fails to mimic eccentricity periodicities longer than 10^6 years (compare black curves, Fig. 7A, C).

Eccentricity Rhythms

The climatic effect of the precessional cycles is modulated as the four eccentricity rhythms introduced by gravitational interactions with Mercury, Venus, Mars, and Jupiter go into and out of phase. In any one case, the largest effect is obtained at the frequency corresponding to the "difference tone" or "combination tone" between them as shown in Table 1B.

←

FIG. 5 (opposite column).—Fine structure of selected 406 ky superbundles, tuned to same length. a–b–c–d, 95 ky cycles in ascending order. In superbundles 13, and 14, transitional to red facies, show precessional signals of low amplitude but high fidelity, and confluence of central bundles. Amplitudes are high but fidelity of preservation is low in cycles 8 and 10, reflecting a strong obliquity signal. In cycle 24 the precessional signal has largely been wiped out by bioturbation. Confluence of the b and c bundles is shown in cycles 13, 14, and 24.

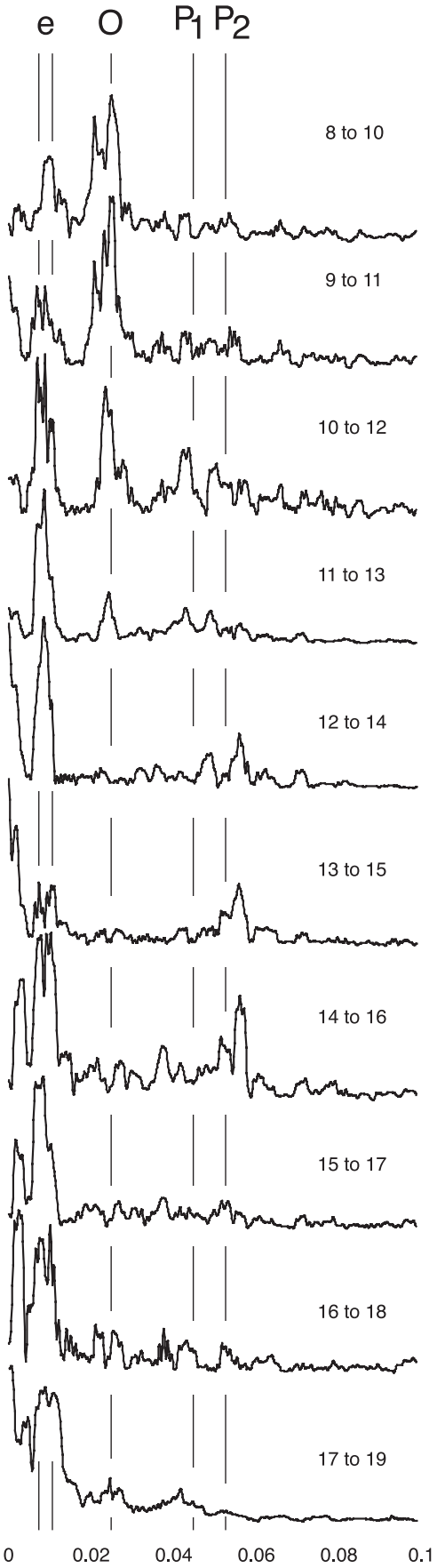

Short-Eccentricity Rhythms.—

The close proximity of the frequencies for the Jupiter–Mars relationship and the Jupiter–Earth relationship combines these in the period for e_1. That between Mars–Venus and Earth–Venus defines e_1. These are the modes of the short-eccentricity rhythm, to which we ascribe the "bundles" of couplets in the Scisti a Fucoidi.

These bundles, generally 30–50 cm thick, conspicuous in outcrop as well as in our logs, are defined by two features. The central couplets in such a bundle are generally more calcareous and more bioturbated, and therefore less sharply differentiated than are those at the boundaries. Also, in the drab facies they are punctuated by PAPs and inferred PAPs, as shown in Figures 4 and 9.

A statistical distribution of PAPs and gray layers (inferred PAPs) (Fig. 9C, D) in a 10 My series is plotted for the 20 precessions of the 406 ky eccentricity cycle. It shows their preferred incidence at bundle boundaries and peak incidence at superbundle boundaries. This distribution of PAPs seems to be largely a primary feature, but the greater proportion of inferred ones in the mid-bundle precessions suggests that the pattern has become somewhat enhanced by the stronger bioturbation in the better-aerated conditions of the mid-bundle region.

The scattering of peaks in the short-eccentricity band of the raw spectrum (Fig. 3A) is logically attributable to "stratigraphic distortion" by varied accumulation rates. That they should be pulled together into a single one by tuning is to be expected, but the period of that peak is a very good match to the predicted one (Fig. 3B, C).

Long-Eccentricity Rhythm.—

The phase relationship between Earth and Jupiter (Table 1B) yields the difference tone of 404.100 ky, the long-eccentricity rhythm, which is very stable. This is the frequency to which we ascribe the superbundle in the Scisti a Fucoidi.

At intervals the bundles of the gray-scale log are clearly grouped into sets of four, the 406-ky-long eccentricity cycle (cycles 10, 13, 16, 24, and 30 in 4 and 8, and in Fig. 16). These superbundles are a larger version of the bundles. They show a similar punctuation by PAPs, a similar confluence of central bundles, and a tendency to be separated by more marly bundles. The intervening bundles do not reveal such grouping, but, as explained above, we found it possible to project the 406 ky cycle through these intervals by assigning every fourth bundle boundary to the superbundle schedule. Three superbundles (7; 27 with the Urbino black marlstone; and 30 with a thick decalcified maroon clay) contain condensed intervals that require 100 ky additions to meet the next superbundle in phase.

Red Shift.—

In the spectra tuned to the 406 ky cycle the e_1 and e_2 eccentricity modes, presently at 94.8 and 123.9 ky (Laskar, 1999, his

←

FIG. 6 (opposite column).—Spectra of 1,200 ky segments (three 406 ky cycle equivalents) as recognized by 406 ky tuning, overlapped. Note the great rise of obliquity power in upper part of core, and the red and blue shifts in the precessional modes. e, modes of short (ca. 95 ky) eccentricity rhythm with which the spectra have been aligned; O, P, astronomically predicted modes of obliquity and precessional rhythms.

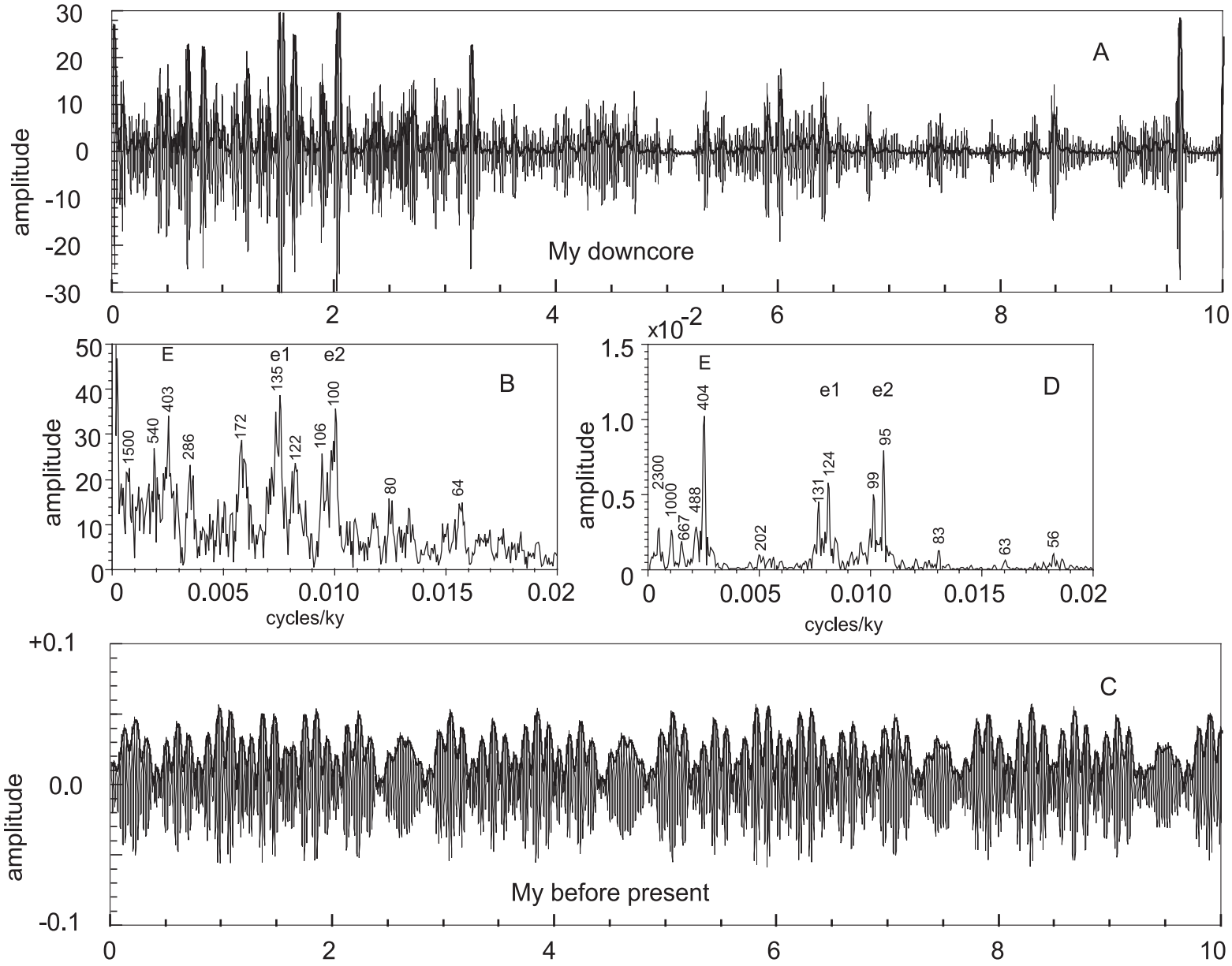

FIG. 7.—Amplitude modulations of precession index. **A)** Precession components of the 406-ka tuned gray-scale scan (gray curve), from top of cycle 8 down, obtained by Taner bandpass filtering with a lower cutoff frequency of 0.035 cycles/ky, and upper cutoff frequency of 0.060 cycles/ky, with a cutoff slope of 15 db/octave. The amplitude modulations were obtained by Hilbert transformation (black curve). **B)** Amplitude spectrum of the amplitude modulation series shown in Part A. **C)** Theoretical precession index over the past 10 million years (gray curve), and eccentricity series (black curve). **D)** Amplitude spectrum of the eccentricity series shown in Part C. Labels indicate periodicity in ky.

table 6), appear significantly "red-shifted" toward lower frequencies (Fig. 10). An overlay of the spectra for the stacked quarter-series, the stacked half-series, and the full series (Fig. 10E) demonstrates the gain in resolution obtained from the longer series, shows this red-shift in all, and establishes the e_1 and e_2 modes at 100.2 and 132.9 ky. Despite the shift, E has remained essentially invariant at 407.2 ky (Fig. 10E), indistinguishable from the present value of 406 ky. On the other hand, it is only spottily clear in the time series, and strong only in the spectrum of the second quarter, where it also appears to be displaced slightly toward lower frequencies.

The explanation for the red-shift in e_1 and e_2 lies in tuning errors. We demonstrate this as follows. In Figure 11A, the "true eccentricity series" (top curve) contains the 406 ky component (middle curve) that we seek to use as a uniform "metronome", through identification of successive 406 ky minima in the gray-scale curve. In tuning the Piobbico series, we identified the 406 ky component primarily through visual identification of bundle boundaries (Figs. 4, 5, 8). However, as shown in Figure 11A (arrows), the minima of the "true" eccentricity series do not occur at precise 406 ky intervals because of interference with the short-eccentricity cycles. In fact, over a 10-million-year simulation, 75% of the local minima of the "true" eccentricity series occur at intervals slightly less than 406 ky. This means that (incorrectly) treating these minima as uniform 406 ky increments, and tuning the series accordingly, effectively "stretches" e_1 and e_2 within the assumed 406 ky increments to slightly longer periodicities (compare the bottom gray and black curves). This is confirmed in the spectra of the original "true" and mistuned "distorted" eccentricity series shown in Figure 11B (top and middle curves).

The "distorted" eccentricity spectrum closely resembles the eccentricity band of the Piobbico series (Fig 10E, middle and bottom curves). Not only is power diverted into virtually the same (lower) frequencies, but additionally, the doublet structure of e_1 is lost, and that of e_2 is broader and less distinct. This nearly identical fine-scale structure in e_1 and e_2 of the Piobbico series and the experimentally distorted eccentricity spectra suggest that the red shift is due to a small systematic error in picking cycle boundaries. Finally, the absence of a sharp 406 ky spectral peak in the tuned Piobbico series suggests that the minima selected in the tuning deviated significantly from those of the true E component in the series.

Longer Periodicities.—

Although the Piobbico series is theoretically long enough to resolve the very long-period AM components at 2.35 My, 967 ky, and 697 ky (Table 1B, Fig. 12D), neither the eccentricity band (Fig.

→

TABLE 1 (opposite column).—The Earth's orbital parameters in terms of the planetary fundamental frequencies. The Earth's axial precession rate is estimated at $k = 50.4712''$/year, which gives a frequency of revolution of 3.8944×10^{-2} cycles/ky (i.e., a period of revolution of 25,678 years). Subscript numbers identify the planet: 1 = Mercury, 2 = Venus, 3 = Earth, 4 = Mars, 5 = Jupiter, and 6 = Saturn; for each of these planets, the fundamental frequencies g_i indicate changes in orbital eccentricity and longitude of perihelion, and s_i indicate changes in orbital inclination and longitude of the ascending node, for the *i*th planet (Laskar 1990). Labels P1, P2, E, e_1, e_2, and O indicate major orbital components labeled in Figures 6, 7, and 8.

A. Precession index

	Fundamental frequency	frequency (cycles/kyr)	period (years)
P_1	$k+g_5$	4.22×10^{-2}	23684
	$k+g_1$	4.33×10^{-2}	23115
	$k+g_2$	4.47×10^{-2}	22373
P_2	$k+g_3$	5.23×10^{-2}	19104
	$k+g_4$	5.28×10^{-2}	18952

B. Amplitude modulations of the precession index

	Fundamental frequency	frequency (cycles/kyr)	period (years)
	g_4-g_3	4.250×10^{-4}	2352900
	g_1-g_5	1.040×10^{-3}	961700
	g_2-g_1	1.435×10^{-3}	697000
E	g_2-g_5	2.475×10^{-3}	404100
e_1	g_3-g_2	7.646×10^{-3}	130800
	g_4-g_2	8.071×10^{-3}	123900
e_2	g_3-g_5	1.012×10^{-2}	98800
	g_4-g_5	1.055×10^{-2}	94800

C. Obliquity oscillations

	Fundamental frequency	frequency (cycles/year)	period (years)
O	$k+s_3$	2.44×10^{-2}	40996
	$k+s_4$	2.52×10^{-2}	39657
	$k+s_6$	1.86×10^{-2}	53714
	$k+s_1$	3.46×10^{-2}	28889

D. Amplitude modulations of the obliquity

Fundamental frequency	frequency (cycles/kyr)	period (years)
s_4-s_3	8.24×10^{-4}	1214174
s_3-s_6	5.78×10^{-3}	173145
s_4-s_6	6.60×10^{-3}	151536
s_1-s_4	9.40×10^{-3}	106394
s_1-s_3	1.02×10^{-2}	97822
s_1-s_6	1.60×10^{-2}	62507

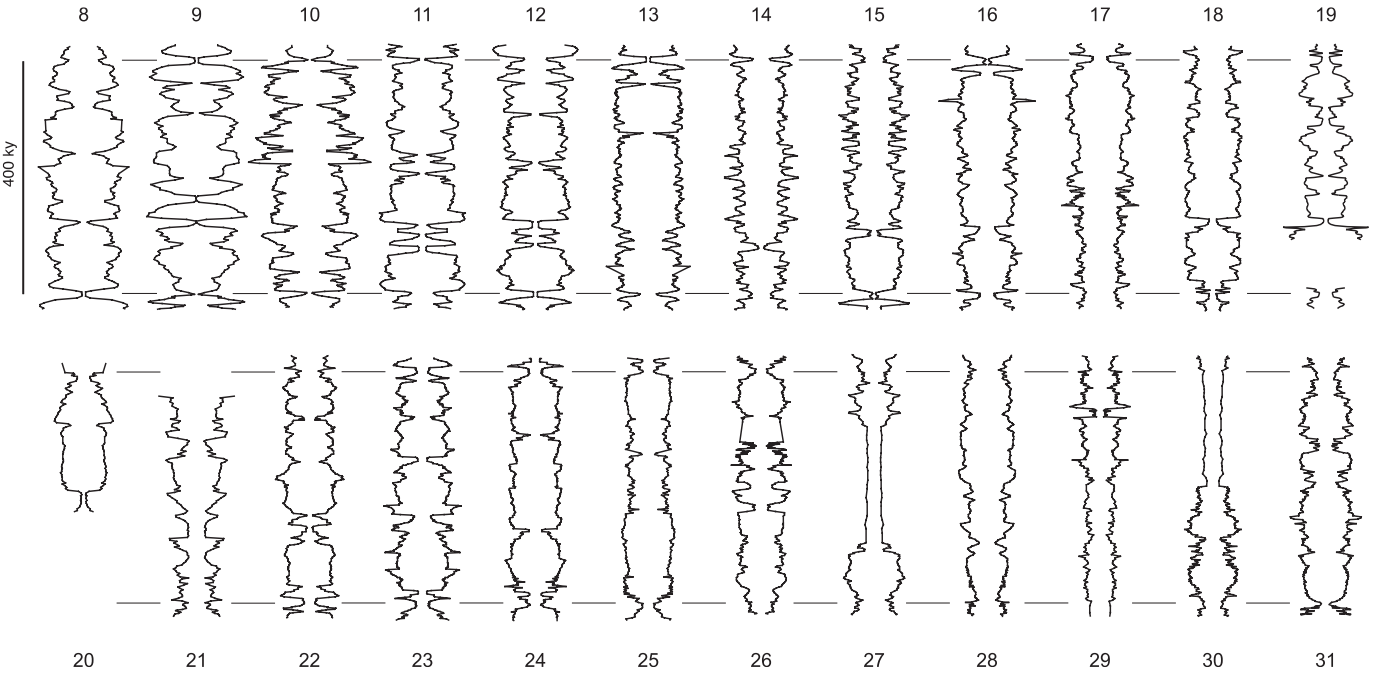

FIG. 8.—Comparison of the successive superbundle signatures in gray-scale log, tuned to 406 ky cycle and numbered from top Albian downward. One 95 ky cycle has been added to the Urbino black shale (superbundle 27), and two to the maroon shale of cycle 30.

3) nor the AM series of the filtered precession (Fig. 7B) show evidence for these periodicities, although the latter indicates a spectral peak at 1.5 My.

An alternative way to search for these AM components is through quadrature analysis of the short eccentricity (Table 1B): e_1 and e_2 are in reality doublets, each of which through time undergoes an amplitude modulation 2.35 My long; the four components comprising e_1 and e_2 together also interact to produce a shorter 406 ky modulation. The filtered short eccentricity of the tuned series is shown along with its AM series in Figure 12A, and their filtered theoretical equivalents in Figure 12C. The AM spectrum of the data (Fig. 12B) reveals major modulation periodicities in the 400 to 580 ky range. Of these, the peak at 400 ky is very sharply defined, and another, broader periodic component occurs at 1.5 My. The peaks at 500–580 ky may reflect tuning errors, i.e., errors in the choice of some of the 406 ky segments that caused one or more (true) 406 ky amplitude modulations to mistakenly be distributed over more than one 406 ky (tuned) period at a time.

Most noteworthy is the absence of the predicted major 2.35 My amplitude modulation (Fig. 12D). This modulation is caused by the interaction between the moving orbital perihelia and eccentricities of Earth and Mars, g4–g3, and has been observed in the short eccentricity in Oligocene–Miocene sediment (Zachos et al. 2001). Here, however, the Piobbico series shows instead a modulation at 1.5 My; this is also present in the AM series of the filtered precession index band (Fig. 7B), presumably the direct stratigraphic expression of the same component. Whether this 1.5 My component is the result of geological distortion to what was originally a 2.35 My modulation, i.e., disruptions by episodic PAPs, or is evidence for a real and significantly different g4–g3 during the mid-Cretaceous will require further investigation. There has been discussion, however, that during the Late Triassic and Early Jurassic, g4–g3 may have had a ca. 1.6 to 1.7 My periodicity (Olsen and Kent, 1999; Hinnov and Park, 1999). This would suggest that the Piobbico 1.5 My component may be a true expression of Cretaceous g4–g3, and that a shift in g4–g3 of astrodynamical significance occurred sometime between late Mesozoic and middle Cenozoic times.

Obliquity Rhythm

Our nearest sister planets affect not only the eccentricity of Earth's orbit but also its axial inclination because of the pull exerted on our equatorial bulge (Table 1C) by planets with an ecliptic notably different from ours. The main period of the self-induced oscillation of 41 ky, while Saturn induces a lesser one at ca. 54 ky. The closely spaced frequencies of the obliquity rhythm also produce amplitude modulations, shown in Table 1D.

The obliquity rhythm comes and goes through the core, as seen in spectra (Fig. 6) and in an extraction of the obliquity signal (the 0.018 to 0.038 ky pass-band) from the gray-scale series (Fig. 13). This inconstancy is attributable not to modulations of the obliquity cycle itself but to the Earth's response. Largely generated in the polar regions, its episodic strength in the mid-latitudes may be largely dependent upon its transmission.

Like the cycles of the precession–eccentricity syndrome, those of the obliquity drove variations in carbonate production and in bottom redox conditions. Thicker and abundant PAPs and relatively pure limestones coincide with the presence of strong obliquity signals in cycles 8–12, suggesting that primary productivity was increased at these times. The changing phase relations between the precession index and the obliquity signal largely mask the visual impression of a 40 ky regularity (Fig. 5).

Interactions among the varying inclinations and ascending nodes of the planetary orbits produce amplitude modulations in the Earth's obliquity variation listed in Table 1D. Because orbital inclination is the most unsteady of the planetary motions, the Earth's obliquity variation is not expected to have remained stable over remote geologic times (Laskar, 1999). Nonetheless,

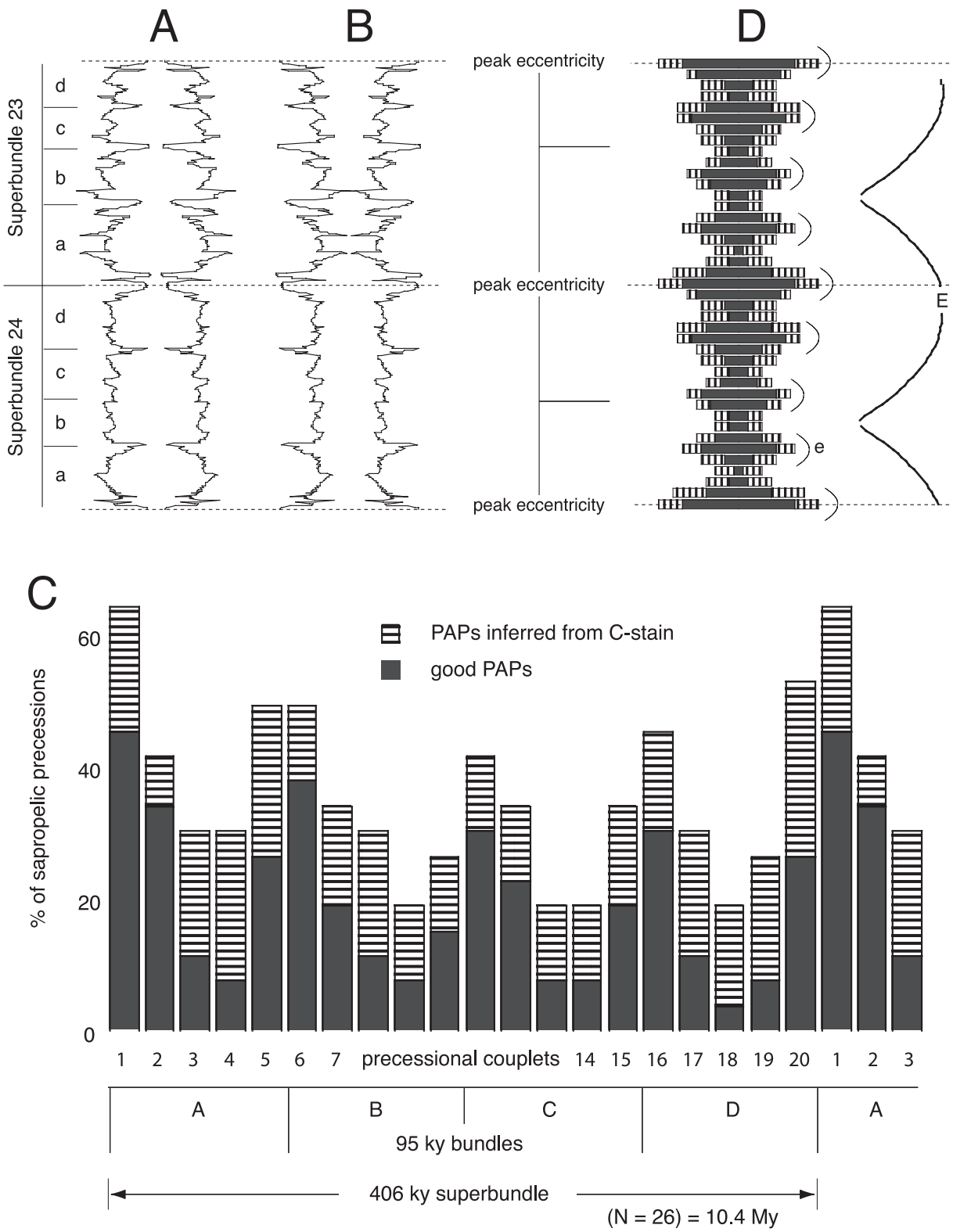

FIG. 9.—PAPs and the phasing of cycles. **A)** Gray-scale curve mirrored on black, yielding an image of carbonate cycles bounded by precessional black pulses (PAPs). **B)** The alternative, mirrored on white, yielding an image of cycles centered on PAPs. **C)** Statistical distribution of PAPs and grayed (PAP-inferred) couplets (precessions) in a stack of 26 406-ky supercycles. Incidence of PAPs in the first precession of each 95 ky cycle would be near 100% but for their absence in the red facies and for a reduction of peaks by a running three-point average. **D)** Patterns of statistical PAP incidence, projected to 800 ky, and suggested phase match to eccentricity cycles.

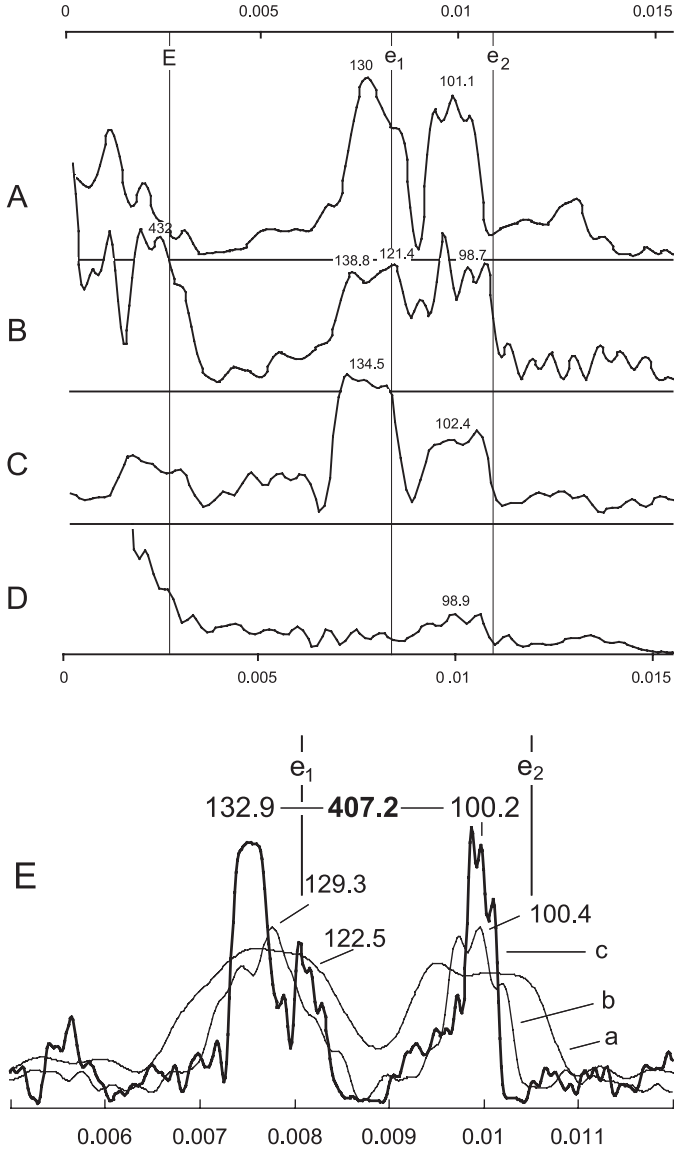

FIG. 10.—Red shift in frequency modes of short eccentricity cycles (e_1, e_2) tuned to 406 ky cycle. E, the 406 ky cycle of eccentricity, is not well resolved in such short series. **A–D)** Power spectra for the four "quarters" of the 10 My core series, tuned to the 406 ky cycle. (cycles 0–13, 14–19, 21–26, 27–31). (Ea) the sum of the above spectra; **E)** comparison of (a) the sum of the four quarter series; (b), the sum of the two half-series spectra; (c), the spectrum for the full series. The frequency modes of the short-eccentricity (e) rhythm have been displaced to 100.2 and 132.9 ky, respectively, but E, their difference tone, remains close to present value of 406 ky.

Figure 13C shows that, in the tuned Piobbico series, spectral power is concentrated at the two main predicted obliquity frequencies, k + s3 = 0.0244 cycles/ky and k + s4 = 0.0252 cycles/ky (see Table 1C), suggesting that s3 and s4 may have been invariant over the past 100 My.

The Piobbico filtered obliquity series (Fig. 13A, B) lacks certain modulations to be expected. There is no dominating 1.2 My modulation that would indicate the presence of predicted s4–s3, nor are there modulations at the 100 ky and 170 ky time scales, also predicted for the obliquity (Figs. 13C, D; Table 1D). This may be attributable to degradation of signals during atmospheric or oceanic transmission of signals from distant sites of generation.. But, if taken at face value, it would suggest that the two obliquity frequencies in Figure 3C cannot be ascribed to s3 and s4 as given in current models (i.e., Laskar, 1999) and that the other s_i are probably different as well.

Instead, broad peaks centered on 242 ky and 133 ky periods (Fig. 13D) characterize the AM spectrum. Whether these peaks reflect true interactions s_i–s_j for the Cretaceous, or irregular amplitude patterns not related to orbital forcing, will require further investigation. Evidence suggests that the s_i during the Jurassic Period were different from those predicted for the past 20 My (Hinnov and Park, 1999). By Oligocene–Miocene times, however, s4–s3 with a 1.2 My variation in the periodicity is clearly visible in obliquity-forced sedimentation (Shackleton et al., 1999; Zachos et al., 2001).

STRATA AND PHASE

How do the stratigraphic cycles—the eccentricity bundles and the precessional couplets—relate to the precession index of Berger and others? The alternatives are shown in Figure 9A, our conventional gray-scale log, and Figure 9B, its inverse. Do PAPs, segmentations in A and spikes in B, represent the lows or the highs of the eccentricity cycles?

In the precession index curve, low eccentricity implies moderate seasonality with little contrast between the perihelial summer phase and the perihelial winter phase of the precession. This pattern finds its match in the damped gray-scale variations characteristic of middle of the bundles. As eccentricity grows, the seasons become more damped in the perihelial winter phase and more extreme in the perihelial summer phase. We take this to be expressed in the higher amplitudes of the precessional signals at bundle boundaries. Accordingly, PAPs were preferentially associated with eccentricity peaks, at the level of both the short and the long eccentricity rhythms. The statistics for their incidence are shown in Figure 9C and their inferred relationship to the eccentricity cycles is shown in Figure 9D. The Quaternary sapropels of the Mediterranean—also PAPs of a sort—are also associated with high eccentricity (Rossignol-Strick, 1985).

Turning to the precessional cycle, we ask whether the PAPs were formed in the phase of perihelial summers or that of perihelial winters. The former, marked by hotter-than-normal summers and colder-than-normal winters, leads to high monsoonality, likely to be expressed in high productivity. The perihelial winter phase, on the other hand, reduces seasonality and monsoons, and presumably favored stable stratification.

This poses the question of whether the PAPs resulted from organic hyperproduction or from exceptional preservation of organic carbon. de Boer (1982, 1983) and de Boer and Wonders (1984) took carbonate productivity to be a function of primary productivity. Herbert et al. (1986) presented evidence for more organic silica in the limestones (versus PAPs and other marls), suggesting higher primary production in the carbonate-rich phase. The microbiota offers further support: limestones denote the times when coccolithophoraceans, part of the phytoplankton, flourished and contained the species generally identified with upwelling and fertility (Erba, 1988, 1992). The richest assemblages of planktonic foraminifera, associated with the marls and PAPs, would seem to have resulted from depth tiering, suggesting a preference for clearer oligotrophic waters (Premoli Silva et al., 1989b).

These observations support the de Boer model, that PAPs represent not productivity but episodes of carbon preservation.

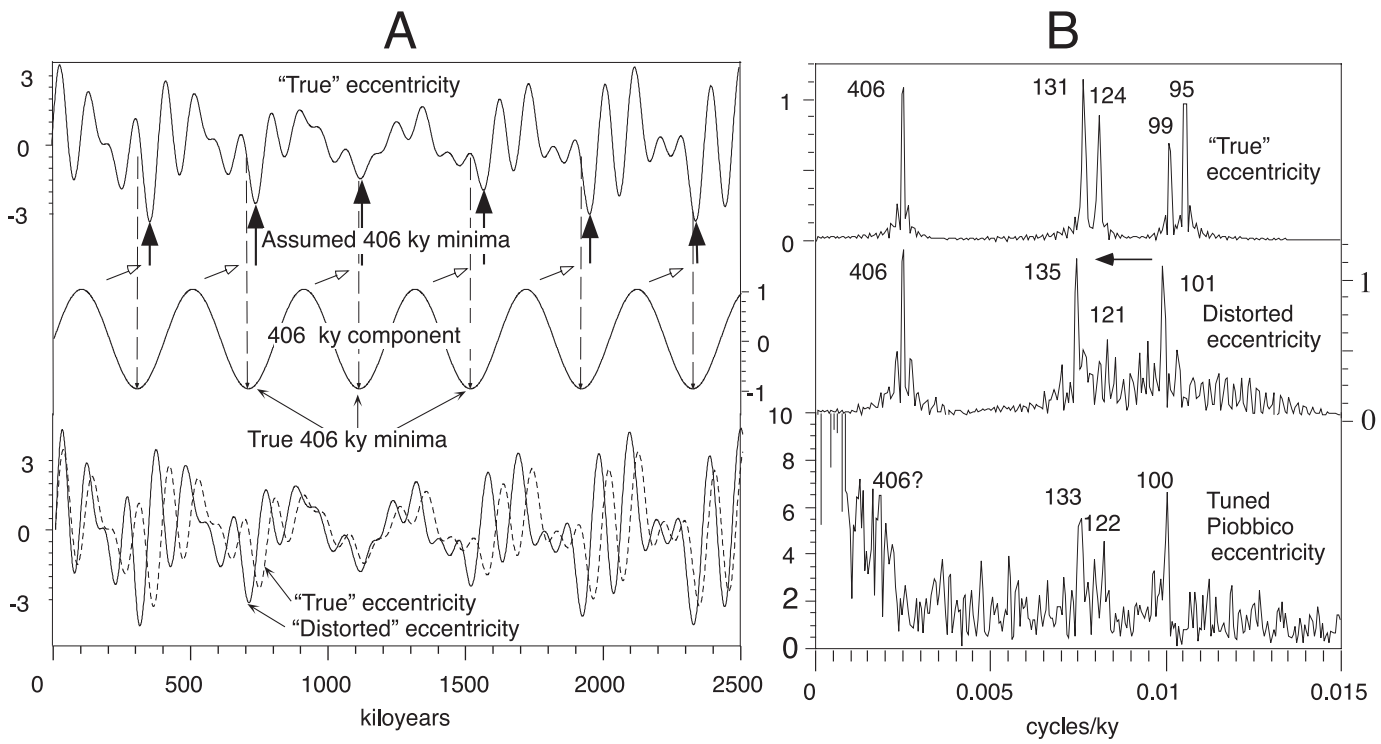

FIG. 11.—**A)** An approximation of the "true" eccentricity, $x(t) = \sin(2\pi t/406) + 0.9\sin(2\pi t/131) + 0.7\sin(2\pi t/124) + 0.6\sin(2\pi t/99) + 0.9\sin(2\pi t/95)$, with minima indicated every ca. 400 ky by heavy black arrows (top curve); the 406 ky component of the "true" eccentricity, i.e., $\sin(2\pi t/406)$ (middle curve), with minima indicated by dashed arrows; and the "true" eccentricity replotted (bottom gray curve) and compared to a "distorted" eccentricity (bottom black curve) obtained by tuning the "true" eccentricity minima to constant 406 ky increments. **B)** The amplitude spectrum of a "true" eccentricity series 10 million years long (top curve), computed as in Part A, of a 10-million-year long "distorted" eccentricity (middle curve) computed as in Part A, and of the eccentricity band of the tuned Piobbico series 9.6 million years long (bottom curve).

Accordingly we assign the PAPs to the perihelial winter phase of the precessional cycle, when seasonality was damped, monsoons were suppressed, hydrodynamics reduced and stratification enhanced. This would seem to differentiate them from the Quaternary sapropels, which originated in the very different hydrodynamic setting of a blind-alley Mediterranean and are thought to represent the high productivity in the perihelial summer phase (Rossignol-Strick, 1985).

PALEOCLIMATIC–PALEOCEANOGRAPHIC INTERPRETATIONS

We think of the greenhouse world as a warmer one in which latitudinal climatic gradients were so low as to have kept permanent ice from reaching sea level and in which ocean temperatures, now near 3°C, hovered around what is now Earth's average surface temperature of ca. 15°C. That is the temperature obtained for Cretaceous ocean bottoms (Douglas and Savin, 1975; papers in Barrera and Johnson, 1999; Huber, Macleod and Wing, 2000).

The ocean is density-stratified. In the present mode, bottom waters are supplied by the cold, though not highly saline, waters of the high latitudes. Chamberlin (1906) reasoned that in greenhouse times the production of such waters would be diminished, while the increased production of dense (saline though warm) waters in the paratropical dry belts would play a competitive role.

As argued by Hay and DeConto (1999), a global "halothermal" circulation of this sort could not have become permanent, lest sequestration of salt in the deep ocean turn the surface brackish. Yet episodic or localized subtropical downwelling of saline waters seems likely. Figure 14, Herrle's (2002) model of this in the Mediterranean Tethys, embodies such downwelling and the very processes that our interpretation of the Scisti a Fucoidi call for.

While global changes in atmospheric and oceanic behavior set the stage for a strong response to orbital forcing, that response is likely to have been heightened by the local geography (Fig. 14). The opening of Tethys to the west, in Jurassic–Cretaceous times, provided an avenue for east–west water transport. It seems likely that trade winds drove warm, saline, nutrient-depleted waters into the westward-narrowing funnel of Tethys, as suggested in Figure 14, and that at times and places such waters of the mixed layer foundered to bottom.

As pointed out by Herrle (2002), the still comparatively aggregated pattern of lands must have left this part of the world particularly liable to orbitally modulated monsoons, which presumably played a large part in local ocean dynamics and elicited strong biotic response.

Drab Facies

The drab facies represents the more prevalent condition, and records sedimentation in a stratified water column, which we

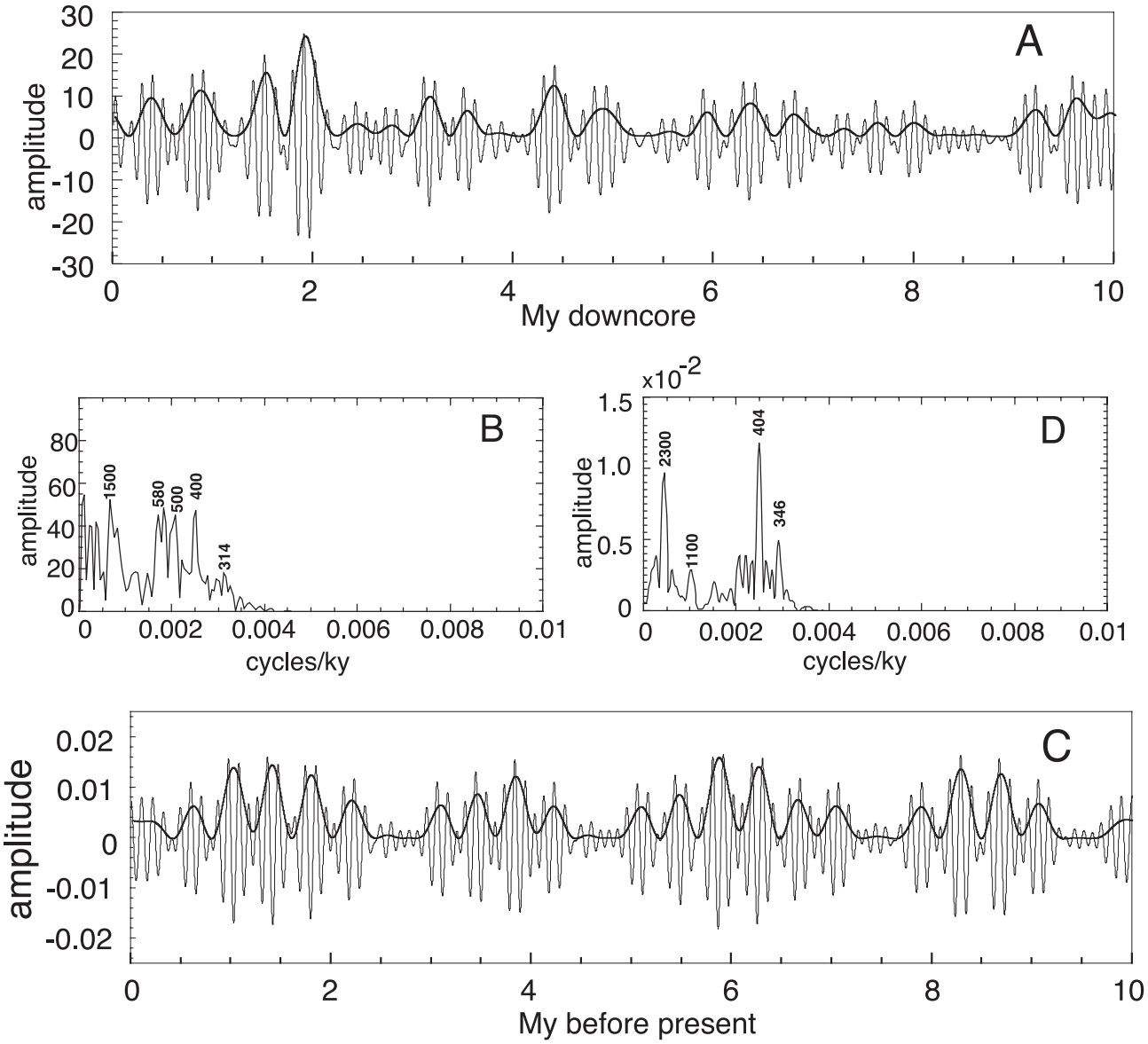

FIG. 12.—Amplitude modulations of eccentricity. **A)** Short-eccentricity components (gray curve) of the 406 ky tuned gray-scale scan, from top of cycle 8 down, obtained by Taner bandpassing with a lower cutoff frequency of 0.007 cycles/ky and an upper cutoff frequency 0.0112 cycles/ky, with roll-off slope of 15 db/octave. Also shown is the amplitude modulation series (black curve), obtained by Hilbert transformation. **B)** Amplitude spectrum of the amplitude modulation series shown in Part A. **C)** Theoretical short-eccentricity components (gray curve) obtained by the same Taner bandpass applied in Part A, and the amplitude modulation series (black curve), obtained by Hilbert transformation. **D)** Amplitude spectrum of the amplitude modulation series in Part C. Labels indicate periodicities in ky.

visualize something like that of the North Pacific. There the oxygen content of surface waters, from 4–6 cm^3/l, drops to a minimum of < 1 cm^3/l at about 1 km, and generally remains below 2 cm^3/l to depths of ca. 2 km, gradually rising to 4–4.5 cm^3/l on the deep bottoms (Dietrich and Ulrich, 1968). In the Albian Tethys, temperatures were higher and shortened reaction rates, while at times orbitally modulated monsoons brought more oxygen to the profile.

We postulate that times of moderate to strong seasonality, associated with the summer perihelion phase of the precessional cycle, generated monsoons, invigorated oceanic circulation, and increased nutrient supply to the surface. This favored coccoliths in the photic zone, yet continued to supply oxygen to the deep bottoms, maintaining a diverse ichnofauna.

The perihelial winter phase, with its reduced seasonality, would have decreased monsoonality and ocean dynamics. This would have brought more oligotrophic conditions to the surface waters, with the clarity that allowed planktonic foraminifera to thrive in depth-zoned communities. It reduced oxygen replenishment, bringing dysaerobic conditions to the bottoms and reducing the ichnofaunas to *Chondrites*. At such times anoxia may well have occurred in an oxygen minimum at lesser depths, but

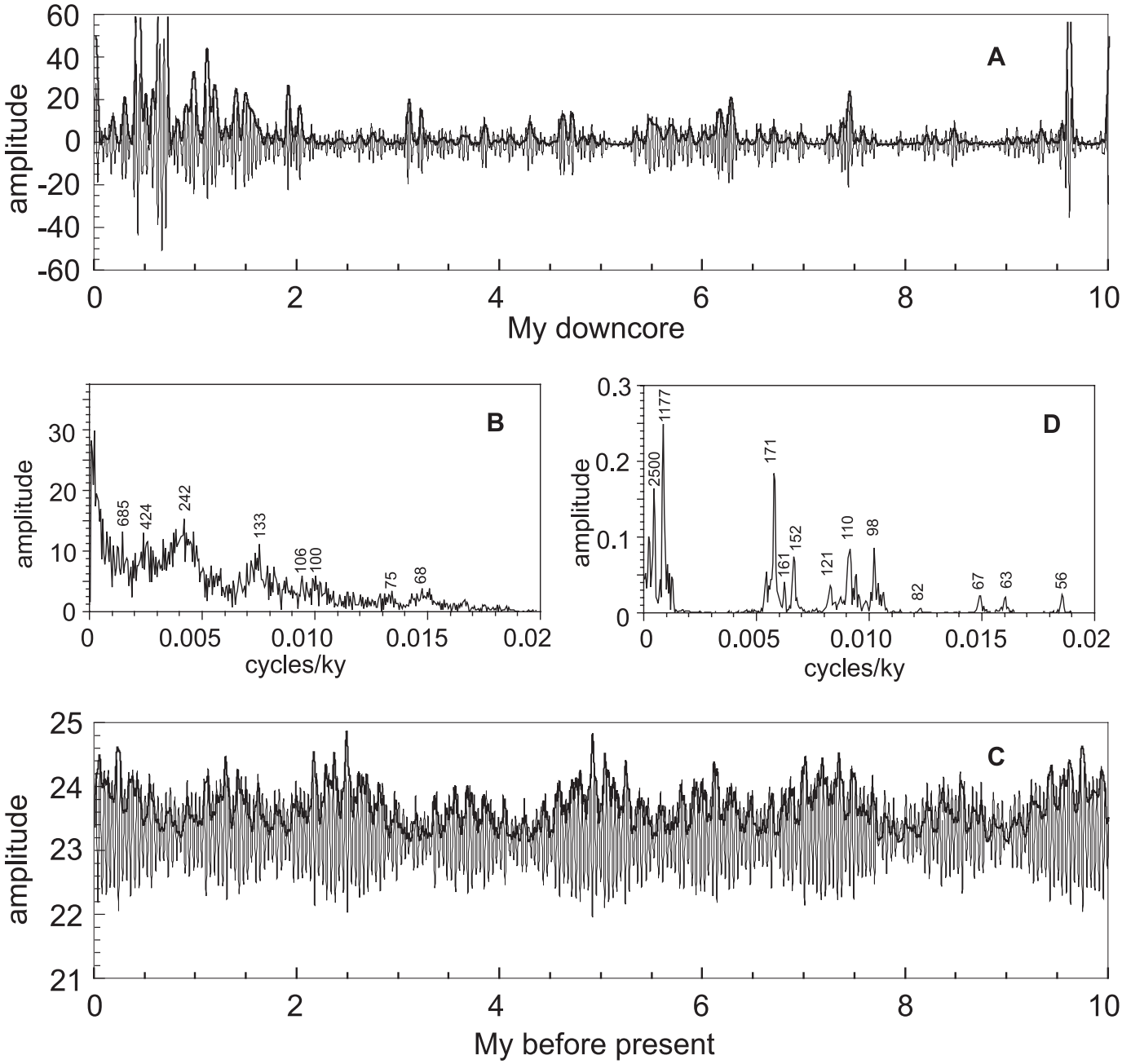

FIG. 13.—Amplitude modulations of obliquity rhythm. **A)** Obliquity components of the gray-scale scan (gray curve), from top of cycle 8 down, obtained by Taner filtering with a lower cutoff frequency of 0.018 cycles/ky and an upper cutoff frequency of 0.038 cycles/ky, with 15 db/octave slope at the cutoffs, and the amplitude modulations (black curve) obtained by Hilbert transformation. **B)** Amplitude spectrum of the amplitude modulation series estimated in Part A. **C)** Theoretical obliquity (gray curve) and its amplitude modulation series (black curve) obtained by Hilbert transformation. **D)** Amplitude spectrum of the theoretical amplitude modulations of the obliquity given in Part C. Labels indicate periodicity in ky.

when magnified by high eccentricity the anoxic zone became extended to the bottom, to form the PAPs.

Red Facies

The persistence of the carbonate cycle in the red facies implies that the upper water regime continued as outlined above, though at somewhat lower carbonate levels (Herbert and Fischer, 1986), implying lower fertility. Deposition at depth occurred in very different, well-aerated waters. These we interpret as Chamberlin's downwelling saline, nutrient-depleted tropical waters, which brought with them their high temperature and relatively high oxygen content. Supply of organic matter, relatively low to begin with, was now further reduced owing to the acceleration of decomposition in the 30°C regime, leaving the deep bottoms depleted in food, while oxidation of sediments would have

proceeded rapidly at those temperatures and would have persisted into early diagenesis occurring within the sediment.

GEOCHRONOLOGY

The Albian Stage is defined, by ammonites, as extending from the base of the *schrammeni* zone (in Tethys, the *tardifurcata*) zone to the end of the *perinflata* zone. In the absence of ammonites we depend on foraminiferal and nannofossil zonation. This does not present a problem at the top of the Albian, where the ammonite-defined boundary nearly coincides with the beginning of the *Rotalipora brotzeni* (= *R. globotruncanoides*) foraminiferal zone. It does present some uncertainty for the base of the Albian, where the ammonite-defined base falls between the first occurrence (FO) of *Predicosphaera columnata* and the FO of *Ticinella primula* (Tornaghi et al., 1989) (Figs. 15, 16).

As noted above, our gray-scale scan allowed us to combine the short and long eccentricity records into an extrapolated count of the more stable 406 ky cycles, which also revealed the need to add a total of 400 ky to condensed zones. This count places the base of the *P. columnata* zone at 30.6 E-cycles for an Albian duration of 12.4 My, 500 ky longer than the calculation by Herbert et al. On the other hand, the appearance of *P. columnata* preceded the beginning of Albian time. In an attempt to move as close to the ammonite-defined base as possible we have placed the boundary midway between the first appearance of *P. columnata* and that of *T. primula* (Figs. 15, 16), at the base of cycle 29 or 11.8 My before the end of Albian time. By chance this closely approximates the 11.9 My figure initially suggested by Herbert et al. (1995). We cannot exclude the possibility that one or two 406 ky cycles are missing.

BROADER IMPLICATIONS

The patterns of orbital cyclicity in the Aptian–Albian Scisti a Fucoidi began in the Tithonian–Neocomian Maiolica Limestone (Herbert, 1992) and lasted, in somewhat degraded form, through the Cenomanian Scaglia Bianca Limestone (Schwarzacher, 1994). In those limestones, carbonate productivity was doubled, which generally doubles the thickness of the couplets and reduces the marly member to a thin interbed, which may or may not be developed as a PAP. Black radiolarian cherts suggest complications.

Precessional redox pulses recorded in organic-matter content, associated with fertility fluctuations in the coccolith flora, have been well documented by Herrle (2002) in the Aptian–Albian hemipelagic deposits of the Vocontian basin of southern France.

Thin black shales and marls, showing remarkable similarity to the PAPs, occur throughout the Early and mid-Cretaceous of the North Atlantic (Dean and Arthur, 1999 and references therein). It thus appears that these precessional fluctuations in planktonic productivity and in bottom redox conditions, modulated by the precession–eccentricity syndrome, were widespread in Tethys.

We suggest that the greenhouse state sensitized the oceans to orbital forcing. Although halothermal circulation at times brought more oxygen into the lower waters of the tropics and subtropics, the lower carrying capacity of the warm waters implies a diminution in the amount of oxygen thus taken down globally, per unit volume of water. It is difficult to judge whether the mean turnover rate of the oceans was higher or lower than the present one, and how it may have varied with orbital forcing, but conceivably

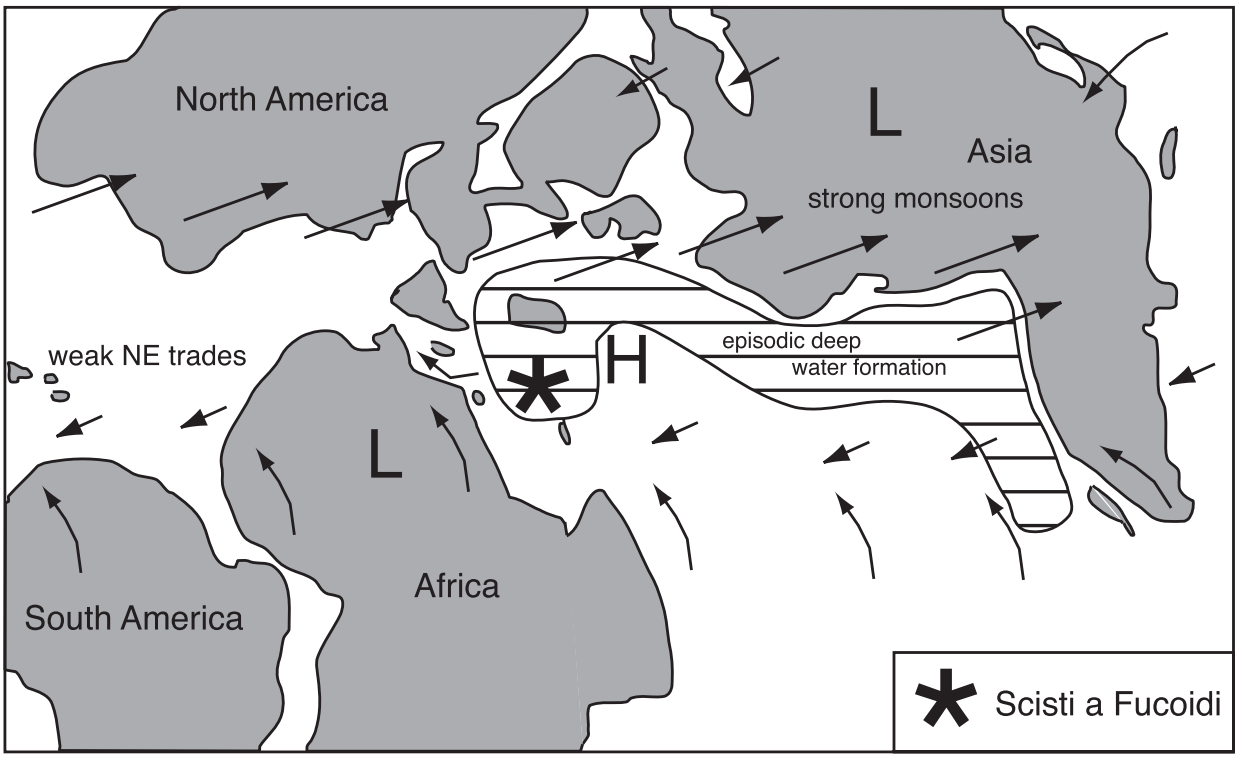

FIG. 14.—Paleogeographic reconstruction for Albian time, showing suggested directions of monsoonal winds and of downwelling warm saline waters. Modified from Herrle (2002), with permission. H, high-pressure area; L, low-pressure area. The star shows hypothetical location of studied sequence.

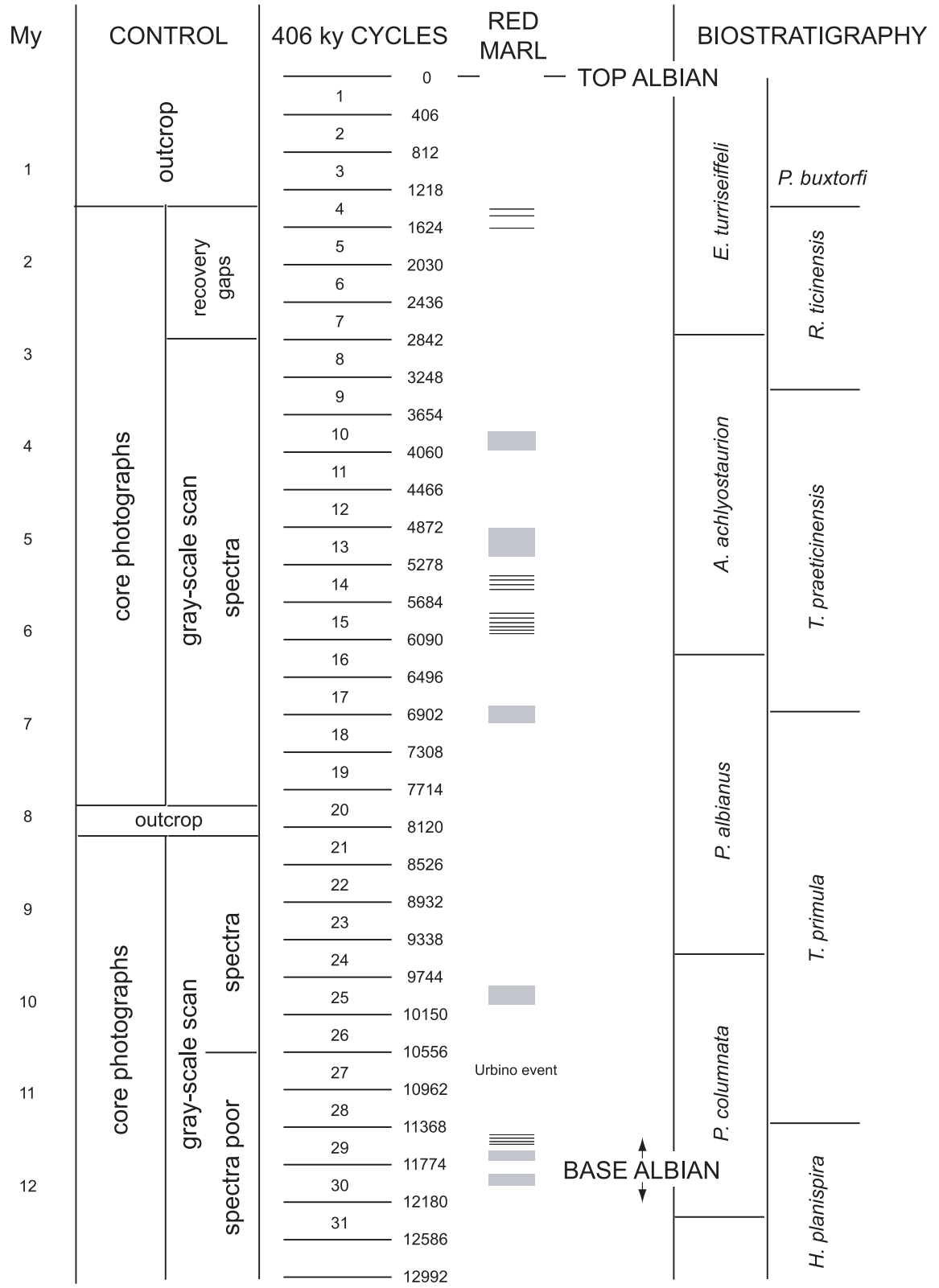

FIG. 15.—Albian cyclochronology as deduced from the Scisti a Fucoidi–Scaglia Bianca sequence in the Apennines of Umbria and Marche (Italy). Observations mainly on Piobbico core, supplemented by data from outcrop (Herbert et al., 1995). Paleontology after Premoli Silva (1977) and Erba (1986, 1988, 1992) and Tornaghi et al. (1989). Duration of the Albian is estimated at 11.9 ± 0.5 My.

the greater role of salinity in circulation slowed the return of some of the deeper waters. All this would have tended to deplete the oxygen content of the mid-water masses.

The high temperatures, implying more rapid decomposition of sinking organic matter, must have intensified the oxygen minimum and at times extended it downward. Consumption of more organic matter in the water column left less for benthic life and for burial the deep-sea sediments.

As pointed out by de Boer (1983), a number of observations suggest an accelerated rate of carbon burial in Early Cretaceous time. These include the episodic formation of large and persistent anoxic water masses (OAEs), the widespread formation of black shales in epeiric seas, and the extraordinary role which this time played in the generation of petroleum (Irving et al., 1974; Tissot, 1979). A corollary to carbon burial is the release of oxygen. Atmospheric oxygen levels at this time may have been higher than present ones, leading to a greater incidence of wildfires, possibly reflected in the high proportion of soot in the Scisti a Fucoidi (Pratt and King, 1986). The possible relation of wildfires to orbital forcing remains to be explored.

As carbon dioxide emissions now move us toward a greenhouse state, we may wonder what lessons the Albian world holds for us. So long as we continue to have extensive ice in the polar regions we shall not come to feel the full brunt of a greenhouse such as the one that developed in Cretaceous time. Furthermore, we are living at a prolonged time of low eccentricity, in which orbital forcing remains moderate. Yet it seems inevitable that some changes in circulation will occur and that the development of higher temperatures in the mid-water masses is bound to accelerate the decomposition of organic matter settling through the water column. This may in places drive the oxygen minimum to critically low levels that could interfere with diurnal migration of organisms which, in the Neogene icehouse, lost the means of coping with such oxygen deficits.

SUMMARY AND CONCLUSIONS

(1) Albian coccolith–globigerinacean marls and limestones of the Umbria–Marche belt (Italian Apennines), deposited at a depth of ca. 2 km, are remarkably cyclic in structure. Building on earlier studies we reanalyzed the Piobbico core with an image-processed photolog and a variety of time series studies designed to follow orbital forcing through ten million years of deep-water sedimentation.

(2) Of two basic facies, we attribute the drab one (white–greenish gray–black) to deposition in a stratified water column, the red one to deposition in downwelling saline (halothermal) waters.

(3) Both reflect oscillations in the composition and vigor of planktonic carbonate producers in the upper waters. These are expressed in ca. 8 cm marl–limestone *couplets.* Abundance and diversity of coccoliths and planktonic foraminifera are antithetic. Coccolith production, with indicators of high fertility, dominated the purer limestones. Abundance and diversity of planktonic foraminifera is greatest in the less-calcareous marls, and implies a preference for oligotrophic conditions.

(4) In the drab facies, this record of oscillations in the upper waters received the overprint of redox oscillations on the bottom. A diverse ichnofauna in the limestones reflects aerated conditions, whereas restriction to *Chondrites* in the marly member of the couplet suggests oxygen deficiency. Episodically this dropped to anoxia, resulting in black marlstones (PAPs, precessional anoxic pulsations).

(5) Such couplets are grouped into ca. 40 cm bundles punctuated by more marly couplets containing PAPs.

(6) The red facies shows similar carbonate fluctuations of somewhat lower carbonate content but lacks the redox cycle except in transitional conditions. Despite deposition in highly aerated settings, it lacks extensive bioturbation, suggesting that supply of organic matter to the bottom was minimal.

(7) To the eye, the Scisti a Fucoidi as seen in outcrop, core, photolog, and gray-scale log reveal cyclicity at two major levels, that of the elementary couplet oscillation, and its ca. 5:1 grouping into PAP-punctuated bundles.

(8) Digitized pictures, converted to a photolog stripped of nonstratigraphic information, served to construct a gray-scale series and gray-scale log. This, by way of spectra tuned to the 406 ky eccentricity cycle, yielded confirmation of the precessional, obliquity, and short and long eccentricity rhythms.

(9) Regarding precessional cyclicity, the elementary doublet cycle, impressive in the field, yielded only marginal spectral results. Low and scattered peaks, though in some intervals appropriately spaced for the two precessional modes, do not come to coincide precisely with the predicted values for the precession. This is due in large part to variations in accumulation rate, below the tuning level of 406 ky. The couplet record also shows extensive damage from bioturbation and, in places, dissolution. But amplitude-modulation analysis of these signals, filtered out of the series, shows the precise eccentricity modulations to be expected, namely the eccentricity frequencies observed, and leaves no doubt as to the precessional origin of the couplets

(10) Signals of the obliquity rhythm are strong in cycles 8–12, where they increased the incidence and thickness of PAPs. They are weaker and not consistently present in the rest of the core.

(11) The short (ca. 95 ky) eccentricity cycles are recorded in the ca. 40 cm bundles of couplets. The low-amplitude gray-scale variations of the middle couplets of such a bundle suggest low eccentricity, whereas the high amplitudes (PAPs) that punctuate bundles would appear to represent eccentricity peaks. The bundles as plotted are thus inverted expressions of the 95 ky cycle.

(12) Such bundles in turn are intermittently grouped into superbundles of four, inverted expressions of the long (406 ky) eccentricity cycles. These are differentiated in the manner of the bundles.

(13) Interpreting the couplets in terms of precessional phases suggests that the summer perihelial phase brought monsoons, fertility that triggered maximal production of coccoliths but limited abundance and variety in planktonic foraminifera. In the drab facies bottoms were moderately well aerated, as attested by bioturbation by a varied ichnofauna. The precessional winter-perihelial phase, of damped seasonality, brought a lessened production of coccoliths but a more abundant and varied foraminiferal fauna, suggesting olig-

otrophic conditions. In the drab facies, bottoms became stressed by lack of oxygen, as evidenced by restriction of bioturbation to *Chondrites*. When this phase coincided with high seasonality, extreme damping of seasonality brought anoxia to the bottoms and resulted in deposition of black marlstones, precessional anoxic pulsations (PAPs).

(14) To derive a chronology for the Albian, we turned to the gray-scale log, where the 95 ky bundles provide a good but not unambiguous record of the short-eccentricity rhythm. The intermittent appearance of the 406 ky cycle sets a framework. Fitting the 95 ky cycles into that frame necessitated the addition of a total of 400 ky, to three intervals of condensed accumulation.

(15) Extrapolating the 406 ky cycle counts in the core to the entire stage, we estimate the length of the Albian at 11.9 ± 0.5 My, short of the radiometric estimate of 13.3 My by Gradstein et al., (1995) but within their confidence limits of 1.7 My. we cannot, however, exclude the possibility that one or two 406 ky cycles are missing.

(16) The sensitivity of these sediments to orbital forcing may reflect in part the complexities of oceanic circulation in a greenhouse world, and in part the increased rate of chemical and bacterial processes at high ocean temperatures.

(17) Factors contributing to orbital sensitivity may have included the location of the region, in a tropical seaway narrowing westward, thus admitting flux of oceanic waters. Proximity to large continental masses implies confrontation of such nutrient-depleted waters with nutrient-rich ones, fluctuating with weathering and runoff. Those factors as well as upwelling and mixing of water masses fluctuated with the orbitally driven variations in monsoonality, highest in the precessional summer phases at times of high eccentricity.

(18) The time seems to have been one of exceptional rates of carbon burial, which implies an exceptional flux of oxygen to the atmosphere. The high proportion of soot in organic matter suggests that this may have found expression in extensive wildfires.

(19) Although the now impending greenhouse state is not likely to reach the strength of the mid-Cretaceous one, it is likely to intensify the oxygen-minimum zone, and may in places come to interfere with the accustomed patterns of diurnal migration.

(20) The photoscan method proved to be an effective means of exploring patterns of cyclicity in a sedimentary sequence.

APPENDIX: THE PHOTOSCAN APPROACH

Many sequences of stratified rocks recorded climatic variations by a variety of parameters, and thereby incorporated into themselves a record of a hierarchy of cycles forced by the Earth's orbital variations. Extracting this record depends on finding efficient ways to measure these variations through the sequence of strata.

The photoscan method measures variations in a bulk property of the sediment—light reflectivity—as a proxy for one or more oscillating compositional variations.

In the Piobbico core the high reflectivity of calcite renders the most calcareous rocks in shades of white (Herbert and Fischer, 1986), whereas the clay minerals with included or adsorbed iron compounds color the marls gray-green, or, when thoroughly oxidized, red. In addition, certain strata are colored black or neutral gray by elemental carbon (lamp black) or organic compounds, and possibly iron sulfides.

The strata recorded in these color variations are planar, and devoid of sedimentary structures save for occasional ripple-drifted and cross-laminated accumulations of radiolarian tests (particles of extreme mobility).

Photolog

To facilitate magnetic studies the core had been drilled in rocks with a dip of 23°. It was split in the dip direction by diamond saw and cut into segments < 30 cm long. Smoothing with 600 grade carborundum and a light acid etch prepared these for photography as 35 mm Ektachrome diapositives (slides). Shortness of the core segments left the images free of the "edge bias" (the lighting gradients so common in core pictures), which readily produces pseudocyclicity in gray-scale scans (Herbert et al., 1999; Thurow and Nederbragt, 1999).

The Ektachrome slides were initially digitized at a pixel density corresponding to 0.8 mm of rock. These files could be concatenated into a single long log-strip, but one that would be full of nonstratigraphic distractions, from coarse bioturbation and the ca. 23° dip to fractures and chipping of the core induced during and after drilling and in extraction and preparation.

In the beginning we corrected the dip in each picture by means of the skew function in Adobe Photoshop®. But time was saved by running the optical scans parallel to the core axis and correcting drilling depth to stratigraphic depth by the factor cos 23° = 0.92.

Digitization allowed us to remove blemishes by image processing. This we initially applied to the full width of the pictures, but clearing a narrow path sufficed to capture the desired information: a time series of successive color pixels representing stratigraphic features only. Along this path we replaced the images of cracks, shadows, pits, and coarse bioturbation with the color of the beds they crossed. The scans of individual core segments were then overlapped wherever possible to concatenate them into a continuous series, broken here and there where core loss left gaps as estimated at the time of drilling. The construction of this colored image was done in Adobe Photoshop®. Once completed, the image was transferred to Adobe Illustrator® for better-quality imaging and compatibility with other files (i.e., the gray-scale time-series file) that had to be successively included. The time series could then be printed as a noise-free Photolog, to any desired format (Fig. 16).

Gray-Scale Series and Log

Such a time series contains two sets of parameters: the stratigraphic depth range of each stratum, and its color, a multidimensional quality. For normal two-dimensional time-series processing we reduced the color to its gray-scale components, though cognizant of the loss of valuable information—the difference between red and gray, an expression of oxidation state.

For conversion of the colored profiles into their gray-scale equivalents we used NIH Image, software provided by NIH as freeware (http://rsb.info.nih.gov/nih-image/index.html). To convert the color series of the individual pictures, using a standard window of 20 cm length, the edited page is selected, copied, and pasted into NIH Image. The graph command then automatically converts color values into a graph of gray-scale values ranging from 0 (white) to 255 (black), pixel by pixel.

THIS IS FRONT OF COLOR FOLDOUT

PAGE 77

FIG. 16 COLOR

THIS IS BACK OF
COLOR FOLDOUT

PAGE 78

THIS PAGE IS BLANK

Recording and Smoothing

Pasting the gray-scale graph into Kaleidagraph® generates pixel values in the Data window. The "create series" option in the Functions menu serves to provide the relative depth for each data point. For example, given a scan segment extending from depth centimeters 300 to 310, these are entered into the "initial value" boxes of the Create Series panel. 200 pixels in this interval implies a "pixel density" of 0.5 mm / pixel, a figure to be entered into the "linear increment" box. The time series can then be smoothed by choosing the most appropriate pixel size, as explained below.

The dip in the core generally provided stratigraphic overlap between successive segments, helping to concatenate the segments accurately.

Conversion resulted in a gray-scale time series of ca. 56,000 pixels, each equivalent to 0.6 mm of rock. In terms of time, at a mean accumulation rate of ca. 4 Bubnoffs (mm / ky) this implies a mean sample spacing of 200 years.

The definition of geologically distorted responses to simple sinusoidal forcing requires denser sampling than the Nyquist rule would suggest. However, the retention of oscillations at frequencies beyond those sought for is costly in computer time and complicates the graph of the gray scale by a clutter of sub-Milankovitch oscillations, a "furriness" that obscures the larger pattern. We therefore changed pixel density to one equivalent to 6 mm of rock, thereby smoothing the gray-scale log. Figures 4 and 16 show the photolog and, alongside, the gray-scale log, in mirrored form, with "black" at the center, in order to increase visual impact.

Spectra and Tuning.—

Subsequent extraction of power spectra, tuning of the time series to given frequencies, etc., has been made possible by the use of the Analyseries© (Paillard et al., 1996). Cyclicities were apparent from visual inspection of the photolog and the corresponding gray-scale log, and were further explored by means of Fourier frequency spectra of the Thompson multi-tapered type. For tuning the time series to specific frequencies we selected the cycle boundaries and located them in the time series. We then expanded or shrank successive sets of the cycles, by adjusting them to a template with an equal number of equispaced boundaries. This new, tuned graphic series was then resampled at equispaced intervals, in an approach toward the Fourier demand of sampling at equal time intervals. This new series, theoretically closer to time than the initial one, provided improved spectra (Figs. 3, 6, 11). Further operations are described in the text.

ACKNOWLEDGMENTS

Our early work on cyclicity in the Italian Cretaceous, including the drilling of the core, was supported by the National Science Foundation. This and the Italian Consiglio Nazionale delle Ricerche supported the drilling and processing of the Piobbico core. Early studies of the core were aided by the American Chemical Society's Petroleum Research Fund and the International Office of the National Science Foundation. The reanalysis of the Piobbico core was supported by the ENI Petroleum Company's AGIP Division. We are most grateful for the support of these organizations.

Lisa Pratt supervised the coring by the skillful CNR drillers and the beginning stages of core description. Core preparation was performed by several students of Premoli Silva at Universitá di Milano. Elisabetta Erba and Maria Emilia Tornaghi contributed a lithologic study of the core, Maurizio Ripepe the computer files and early computer studies. Discussions with Giovanni Napoleone and Andrea Albianelli engaged in studies of the core's magnetic structure, with Elisabetta Erba, studying the nannoflora, and with Maurizio Orlando and Luciano Gorla of AGIP have proved most rewarding. We thank them all for their participation and aid.

REFERENCES

Barrera, E., and Johnson, C.C., eds., 1999, Evolution of Cretaceous Ocean–Climate Systems: Geological Society of America, Special Paper 332, 445 p.

Beaudoin, B., M'Ban, E.P., Montanari, A., and Pinault, M., 1996, Lithostratigraphie haute résolution (< 20 ka) dans le Cénomanien du bassin d'Ombrie-Marches (Italie): Académie des Sciences (Paris), Comptes Rendus, v. 323, no. 2a, p. 689–696.

Berger, A., 1989, Pre-Quaternary Milankovitch frequencies: Nature, v. 342, p. 133

Berger, A., Loutre, M.F., and Dehant, V., 1989, Influence of the changing lunar orbit on the astronomical frequencies of Pre-Quaternary insolation patterns: Paleoceanography, v. 4, p. 555–564.

Bromley, R.G., and Ekdale, A.A., 1984, *Chondrites*, a trace-fossil indicator of anoxia in sediments: Science, v. 224, p. 872–874.

Chamberlin, T.C., 1906, On a possible reversal of deep-sea circulation and its influence on geologic climates: Journal of Geology, v. 14, p. 363–373.

Cresta, S., Monechi, S., and Parisi, G., 1989, Stratigrafia del Mesozoico e Cenozoico nell'area Umbro-Marchigiana: Memorie Descrittive della Carta Geologica d'Italia, v. XXXIX, 185 p.

Dean, W.E., and Arthur, M.A., 1999, Sensitivity of the North Atlantic Basin to cyclic climatic forcing during the Early Cretaceous: Journal of Foraminiferal Research, v. 29, p. 465–486.

de Boer, P.L., 1982. Cyclicity and storage of organic matter in Middle Cretaceous pelagic sediment, *in* Einsele, G., and Seilacher, A., eds., Cyclic and Event Stratification: New York, Springer Verlag, p. 456–474.

de Boer, P.L., 1983, Aspects of Middle Cretaceous pelagic sedimentation in southern Europe: production and storage of organic matter, stable isotopes and astronomic influences: Geologica Ultraiectina, Utrecht, v. 31, 112 p.

de Boer, P.L., and Wonders, A.A.H., 1984, Astronomically induced rhythmic bedding in Cretaceous pelagic sediments near Moria (Italy), *in* Berger, A.L., Imbrie, J., Hays, J., Kukla, G., and Saltzmann, B., eds., Milankovitch and Climate: Dordrecht, The Netherlands, D. Reidel, p. 177–190.

DeConto, R.M., Brady, E.C., Bergengren, J., and Hay, W.W., 2000, Late Cretaceous climate, vegetation, and ocean interactions, *in* Huber, B.T., Macleod, K.G., and Wing, S., eds., Warm Climates in Earth History: Cambridge, U.K., Cambridge University Press, p. 276–296.

Dietrich, G., and Ulrich, J., 1968, Atlas zur Ozeanographie: Bibliographisches Institut Mannheim, Germany, p. 40.

Douglas, R.G., and Savin, S.M., 1975, Oxygen and carbon isotope analyses of Tertiary and Cretaceous microfossils from Shatsky Rise and other sites in the North Pacific Ocean, *in* Gardner, J.V., ed., U.S. Government Printing Office, Washington, D.C., Initial Reports of the Deep Sea Drilling Project, v. 32, p. 509–520.

Erba, E., 1986, I nannofossili calcarei nell'Aptiano–Albiano (Cretacico inferiore): Biostratigrafia, paleoceanografia e diagenesi degli Scisti a Fucoidi del pozzo Piobbico (Marche): Ph.D. Dissertation, Università degli Studi di Milano, 313 p.

Erba, E., 1988, Aptian–Albian calcareous nannofossils biostratigraphy of the Scisti a Fucoidi cored at Piobbico (central Italy): Rivista Italiana di Paleontologia e Stratigrafia, v. 94, p. 249–284.

ERBA, E., 1992, Calcareous nannofossil distribution in pelagic rhythmic sediments (Aptian–Albian Piobbico core, Central Italy): Rivista Italiana di Paleontologia e Stratigrafia. v. 97, p. 455–484.

ERBA, E., AND PREMOLI SILVA, I., 1994, Orbitally driven cycles in trace-fossil distribution from the Piobbico core (Late Albian, central Italy), *in* de Boer, P.L., and Smith, D.G., eds., Orbital Forcing and Cyclic Sequences: International Association of Sedimentologists, Special Publication 19, p. 211–226.

FIET, N., BEAUDOIN, B., AND PARIZE, O., 2001, Lithostratigraphic analysis of Milankovitch cyclicity in pelagic Albian deposits of central Italy: implications for the duration of the stage and substages: Cretaceous Research, v. 22, p. 265–275

FISCHER, A.G., HERBERT, T.D., NAPOLEONE, G., PREMOLI-SILVA, I., AND RIPEPE, M., 1991, Albian pelagic rhythms (Piobbico Core): Journal of Sedimentary Petrology, v. 61, no. 7 (Special Issue), p. 1164–1172.

GRADSTEIN, F.M., AGTERBERG, F.P., OGG, J.G., HARDENBOL, J., VAN VEEN, P., THIERRY, J., AND HUANG, Z., 1995, A Triassic, Jurassic and Cretaceous Time Scale, *in* Berggren, W.A., Kent, D.V., Aubry, M.-P., and Hardenbol, J., eds., Geochronology, Time Scales and Global Stratigraphic Correlation: SEPM, Special Publication 54, p. 95–126.

HAY, W.W., AND DECONTO, R., 1999, Comparison of modern and Late Cretaceous meridional energy transport and oceanology, *in* Barrera, E., and Johnson, C.C., eds., 1999, Evolution of Cretaceous Ocean–Climate Systems: Geological Society of America, Special Paper 332, p. 283–300.

HERBERT, T.D., 1992, Paleomagnetic calibration of Milankovitch cyclicity in Lower Cretaceous sediments: Earth and Planetary Science Letters, v. 112, p. 15–28.

HERBERT, T.D., AND FISCHER, A.G., 1986, Milankovitch climatic origin of mid-Cretaceous black shale rhythms in central Italy: Nature, v. 321, p. 739–743.

HERBERT, T.D., GEE, J., AND DIDONNA, S., 1999, Precessional cycles in Upper Cretaceous pelagic sediment of the South Atlantic: Long-term patterns from high frequency climate variations, *in* Barrera, E., and Johnson, C.C., eds., Evolution of the Cretaceous Ocean–Climate System: Geological Society of America, Special Paper 332, p. 105–220.

HERBERT, T.D., PREMOLI SILVA, I., ERBA, E., AND FISCHER, A.G., 1995, Orbital chronology of Cretaceous–Paleocene marine sediments, *in* Berggren, W.A., Kent, D.V., Aubry, M.-P., and Hardenbol, J., eds., Geochronology, Time Scales and Global Stratigraphic Correlation: SEPM, Special Publication 54, p. 81–94.

HERBERT. T.D., STALLARD, R.F., AND FISCHER, A.G., 1986, Anoxic events, productivity rhythms and the orbital signature in a mid-Cretaceous deep-sea sequence from Central Italy: Paleoceanography, v. 1, p. 495–506.

HERRLE, J.O., 2002, Paleoceanographic and paleoclimatic implications on mid-Cretaceous black shale formation in the Vocontian basin and the Atlantic: evidence from calcareous nannofossil and stable isotopes: Tübinger Mikropaläontologische Mitteilungen, v. 27, 114 p.

HINNOV, L.A., 2000, New perspectives on orbitally forced stratigraphy: Annual Review of Earth and Planetary Sciences, v. 28, p. 419–475.

HINNOV, L.A., AND PARK, J., 1999, Strategies for assessing Early–Middle (Pliensbachian–Aalenian) Jurassic cyclochronologies: Royal Society (London), Philosophical Transactions, Series A, v. 357, p. 1831–1859.

HINNOV, L.A., SCHULZ, M., AND YIOU, P., 2002, Interhemispheric space–time attributes of the Dansgaard–Oeschger oscillations between 0–100 ka: Quaternary Science Reviews, v. 21, p. 1213–1228.

HUBER, B.T., MACLEOD, K.G., AND WING, S. L., EDS., 2000, Warm Climates in Earth History: Cambridge, U.K., Cambridge University Press, 462 p.

IRVING, E., NORTH, F.K., AND COUILLARD, F., 1974, Oil, climate and tectonics: Canadian Journal of Earth Sciences, v. 11, p. 1–15.

JENKYNS, H.C., 1980, Cretaceous anoxic events: from continents to oceans: Geological Society of London, Journal, v. 137, p. 275–291.

LASKAR, J., 1999, The limits of Earth orbital calculations for geological time-scale use: Royal Society (London), Philosophical Transactions, Series A, v. 357, p. 1735–1759

MANN, M.E., AND LEES, J.M., 1996, Robust estimation of background noise in signal detection in climatic time series: Climatic Change, v. 35, p. 409–455.

OLSEN, P.E., AND KENT, D.V., 1999, Long-period Milankovitch cycles from the Late Triassic and Early Jurassic of eastern North America and their implications for the calibration of the Early Mesozoic timescale and the long term behavior of the planets: Royal Society (London), Philosophical Transactions, Series A, v. 357, p. 1761–1786.

PAILLARD, D., LABEYRIE, L., AND YIOU, P., 1996, Macintosh program performs time-series analysis: Internet program referenced to Eos, Transactions, American Geophysical Union, v. 77, p. 379.

PARK, J., D'HONDT, S.L., KING, J.W., AND GIBSON, G., 1993, Late Cretaceous precessional cycles in double-time: a warm-Earth Milankovitch response: Science, v. 261, p. 1331–1334.

PARK, J., AND HERBERT, T.D., 1987, Hunting for paleoclimatic periodicities in a geologic time series with an uncertain scale: Journal of Geophysical Research , v. 92, p. 14,027–14,040.

PRATT, L.M., AND KING, J.D., 1986, Variable marine productivity and high eolian input recorded by rhythmic black shales in mid-Cretaceous pelagic deposits from central Italy: Paleoceanography, v. 1, p. 507–522.

PREMOLI SILVA, I., 1977, Upper Cretaceous–Paleocene magnetic stratigraphy at Gubbio, Italy: II—Biostratigraphy: Geological Society of America, Bulletin, v. 88, p. 367–389.

PREMOLI SILVA, I., ERBA, E., AND TORNAGHI, M.E., 1989a, Paleoenvironmental signals and changes in surface fertility in Mid-Cretaceous C-org-rich pelagic facies of the Fucoid Marls (central Italy): Géobios, Mémoire Spécial, v. 11, p. 225–236, 6 figs., 3 tables, Lyon.

PREMOLI SILVA, I., TORNAGHI, M.E., AND RIPEPE, M., 1989b, Planktonic foraminiferal distribution records productivity cycles: evidence from the Aptian–Albian Piobbico core (Central Italy): Terra Nova, v. 1, p. 443–448.

PREMOLI SILVA, I., AND SLITER, W.V., 1995, Cretaceous planktonic foraminiferal biostratigraphy and evolutionary trends from the Bottaccione section, Gubbio, Italy: Palaeontographica Italica, v. 82, p. 1–89.

PRETO, N., HINNOV, L.A., HARDIE, L.A., AND DE ZANCHE, V., 2001, A Middle Triassic orbital signature recorded in the shallow-marine Latemar carbonate buildup (Dolomites, Italy): Geology, v. 29, p. 1123–1126.

RIPEPE, M., AND FISCHER, A.G., 1991, Stratigraphic rhythms synthesized from orbital variations, *in* Franseen, E.K., Watney, W.L., Kendall, C.G.St.C., and Ross, W., eds., Sedimentary Modeling: Computer Simulations and Methods for Improved Parameter Definition: Kansas Geological Survey, Bulletin, 233, p. 335–344.

ROSSIGNOL-STRICK, M., 1985, Mediterranean Quaternary sapropels, and immediate response of the African monsoon to variation of insolation: Palaeogeography, Palaeoclimatology, Palaeoecology, v. 49, p. 237–263.

SAVRDA, C.E., AND BOTTJER, D.J., 1994, Ichnofossils and ichnofabrics in rhythmically bedded pelagic–hemipelagic carbonates: recognition and evaluation of benthic redox and scour cycles, *in* de Boer, P.L., and Smith, D.G., eds., Orbital Forcing and Cyclic Sequences: International Association of Sedimentologists, Special Publication 19, p. 195–210.

SCHWARZACHER, W., 1953, Cyclostratigraphy and the Milankovitch Theory: Amsterdam, Elsevier, 225 p.

SCHWARZACHER, W., 1994, Cyclostratigraphy of the Cenomanian in the Gubbio district, Italy, a field study, *in* de Boer, P.L., and Smith, D.G., eds., Orbital Forcing and Cyclic Sequences: International Association of Sedimentologists, Special Publication, 19, p. 87–98.

SCHWARZACHER, W., AND FISCHER, A.G., 1982, Limestone–shale bedding and perturbations of the earth's orbit, *in* Einsele, G., and Seilacher, A., eds., Cyclic and Event Stratification: New York, Springer-Verlag, p. 72–95.

SHACKLETON, N.J., CROWHURST, S.J., WEEDON, G.P., AND LASKAR, J., 1999, Astronomical calibration of Oligocene–Miocene time: Royal Society (London), Philosophical Transactions, Series A, v. 357, p. 1907–1930.

THUROW, J., AND NEDERBRAGT, A.J., 1999, Cretaceous laminated sediments as climate archive (abstract): European Union of Geosciences 10, Strasbourg, France, Abstract volume, p. 225.

TISSOT, B., 1979, Effects of prolific petroleum source rocks and major coal deposits caused by sea-level changes: Nature, v. 277, p. 463–465.

TORNAGHI, M.E., PREMOLI SILVA, I., AND RIPEPE, M., 1989, Lithostratigraphy and planktonic foraminiferal biostratigraphy of the Aptian–Albian "Scisti a Fucoidi", Piobbico core, Marche, Italy: background for cyclostratigraphy: Rivista Italiana di Paleontologia e Stratigrafia, v. 95, p. 223–264.

ZACHOS, J.C., SHACKLETON, N.J., REVENAUGH, J.S., PÄLIKE, H., AND FLOWERS, B.P., 2001, Climate response to orbital forcing across the Oligocene–Miocene boundary: Science, v. 292, p. 474–478.